Effects of Methyl Branching on the Properties and Performance of Furandioate-Adipate Copolyesters of Biobased Secondary Diols

Alastair Little,[a] Alessandro Pellis,[a,b] James Comerford,[a] Edwin Naranjo-Valles,[c] Nema Hafezi,[c] Mark Mascal*[c] and Thomas J. Farmer*[a]

[a]Green Chemistry Centre of Excellence, Department of Chemistry, The University of York, Heslington, YO10 5DD, York, United Kingdom.
[b]University of Natural Resources and Life Sciences, Vienna, Department of Agrobiotechnology, Institute of Environmental Biotechnology, Konrad-Lorenz Straβe 20, 3430, Tulln an der Donau, Austria
[c]Department of Chemistry, University of California Davis, 1 Shields Avenue, Davis, CA 95616, USA

**Corresponding Author E-mail: thomas.farmer@york.ac.uk and mark.mascal@ucdavis.com*

Electronic Supplementary Information

43 pages, 73 figures, 10 tables

Content

S1. Initial Investigation Into Synthesis of Furandioate-Adipate Copolyesters with 2,5-Hexanediol (2,5-HDO) S2
S2. Oxolane Formation Observed in Dean-Stark Distillate S4
S3. [1]H-NMR Spectra of Polyesters, Including End-Group Analysis S7
S4. Chromatograms from GPC Analysis of Copolyesters S19
S5. Literature Values for GPC and DSC Analysis of Known Polyesters S22
S6. DSC Analysis of Copolyesters S23
S7. Visual Appearance of Polyesters from Optimised Reaction Conditions S35
S8. Thickness of Films Prepared S37
S9. Tensile Property Study of Polyester Films S38
S10. Trends in Water Contact Angle vs Furan Content and Polyester Chain Length S42
S11. Polyester Synthesis Using CaLB Enzyme as Catalyst S43
S12. References S43

S1. Initial Investigation Into Synthesis of Furandioate-Adipate Copolyesters with 2,5-Hexanediol (2,5-HDO)

Table S1. Initial Synthesis of Furandioate-Adipate Copolyesters with 2,5-Hexanediol (2,5-HDO)

Entry	Polymer	F:D[a]	M_n[b] / kDa	M_w[b] / kDa	Đ[b]	T_g[c] / °C	Yield[d] / %	Appearance
1	2,5-PHA	0.00	25	38	1.5	-37	81	Beige, sticky, stretchy gum
2	2,5-PHAF0.3	0.30	4.2	6.9	1.7	-24	64	Amber, sticky, viscous liquid
3	2,5-PHAF0.4	0.39	3.9	6.8	1.7	-15	66	Golden brown, sticky, viscous liquid
4	2,5-PHAF0.5	0.54	4.2	8.5	2.0	-1	79	Golden brown, sticky, tacky solid
5	2,5-PHAF0.6	0.58	1.0	2.9	2.8	-7	62	Golden brown, sticky, deformable solid
6	2,5-PHAF0.7	0.72	3.7	7.0	1.9	14	89	Golden brown, hard, tough solid
7	2,5-PHAF0.8	0.81	0.7	1.5	2.5	4	48	Caramel brown, hard, tough solid
8	2,5-PHAF0.9	0.83	0.8	1.8	2.3	0	59	Caramel brown, hard, tough solid
9	2,5-PHF	1.00	1.0	2.1	2.2	22	57	Rust red, hard, brittle, glassy solid

[a] Furandioate:total diester molar ratios of the copolymer formed, where F = furandioate and D = furandioate + adipate, determined by ^{1}H NMR spectroscopy. [b] Determined by GPC. [c] Determined by DSC. [d] Determined from mass formed, assuming removal of all ethanol and excess diol. Reaction conditions: as stated in main manuscript for 1° alcohol conditions.

Table S2. Catalyst Screen for 2,5-PHAF0.7 Synthesis.

Entry	Catalyst	M_n[a] / kDa	M_n[a] / kDa	Đ[a]	Yield[b] / %	Appearance
1	$Zr(O^iPr)_4$	0.7	1.2	1.6	36	Orange, viscous liquid
2	$Ti(acac)_4$	1.3	1.8	1.3	22	Orange, soft, sticky solid
3	Bi_2O_3	1.5	2.8	2.0	79	Yellow, tacky solid
4	$Ti(O^iPr)_4$	3.7	7.0	1.9	89	Orange, hard, tough solid
5	Sb_2O_3	3.9	8.4	2.1	84	Grey, hard, tough solid

[a] Determined by GPC. [b] Determined from mass formed, assuming removal of all ethanol and excess diol. Reaction conditions: as stated in main manuscript for 1° alcohol conditions.

Table S3. Years Remaining of Known Reserves of Each Metal Used Catalyst Screen.[1]

Element	Remaining years until depletion of known reserves
Zr	50 – 100
Bi	5 – 50
Ti	>500
Sb	5 – 50

Table S4. The Hazards of $Ti(O^iPr)_4$ and Sb_2O_3. Data Taken from Sigma-Aldrich.[2, 3]

Catalyst	Hazards
$Ti(O^iPr)_4$	H226 - Flammable liquid and vapour
	H319 - Causes serious eye damage
	H336 - May cause drowsiness or dizziness
Sb_2O_3	H351 - Suspected of causing cancer

Table S5. The Effects of Varying Catalyst Concentration, Amount of 2,5-HDO Diol Added and Time of Diethyl Adipate (DEA) addition.

Entry	Diol : Diester feed ratio	$Ti(O^iPr)_4$ / %mol	Time DEA added / h	M_n[a] / kDa	M_w[a] / kDa	Đ[a]	Yield[b] / %
1	1.25 : 1	1	2	3.7	7.0	1.9	89
2	1.25 : 1	2	2	2.4	4.5	1.9	77
3	2.5 : 1	2	2	1.2	2.7	2.2	87
4	2.5 : 1	2	0	1.4	3.2	2.4	86
5	1.25 + 0.5 : 1	1 + 1	2	1.6	4.0	2.5	77

[a] Determined by GPC. [b] Determined from mass recovered, assuming removal of all ethanol and excess diol. [c] Second addition of 2,5-HDO diol (0.5 mol equivalent to total diester) and catalyst added prior to application of vacuum. Reaction conditions: as stated in main manuscript for 1° alcohol conditions except for changes stated in table.

Table S6. Effects of Increasing Polycondensation Time ($T_{polycond}$).

Entry	$T_{polycond}$ / h	M_n[a] / kDa	M_w[a] / kDa	Đ[a]	Yield[b] / %	Appearance
1	20	1.0	2.9	2.8	62	Golden brown, tough, sticky solid
2	35	1.6	3.1	1.9	38	Black, deformable, sticky solid

[a] Determined by GPC. [b] Determined from mass formed, assuming removal of all ethanol and excess diol. Reaction conditions: as stated in main manuscript for 1° alcohol conditions except for changes stated in table.

Table S7. Effects of Increasing the Time Before DEA Addition (entries 1 vs 2) and Increasing Diol Excess (entries 2 to 6).

Entry	**Diol : Diester feed ratio**	**Time DEA added / h**	**M_n[a] / kDa**	**M_w[a] / kDa**	**Đ[a]**	**Yield[b] / %**
1	1.25 : 1	2	3.7	7.0	1.9	88
2	1.25 : 1	4	2.8	4.9	1.8	84
3	2 : 1	4	14	22	1.6	91
4	2.5 : 1	4	15	22	1.5	81
5[c]	2.5 : 1	4	10	16	1.5	87
6	3 : 1	4	12	17	1.5	96

[a] Determined by GPC. [b] Determined from mass formed, assuming removal of all ethanol and excess diol. [c] Double amount (2 mol%) of $Ti(O^iPr)_4$ catalyst. Reaction conditions: as stated in main manuscript for 1° alcohol conditions except for changes stated in table.

Optimum conditions selected for polymerisations involving secondary alcohol diols:

Diol : diester ratio of 2.0 : 1.0; catalyst loading of 1 mol% with respect to the total moles of diester; 4 h reaction of diol and FDEE prior to addition of DEA; total reaction time dictated by onset of Weissenberg effect. These conditions were used in the synthesis of all copolyesters involving secondary alcohols (2,5-HDO, 1,4-PDO and 2,7-ODO).

S2. Oxolane Formation Observed in Dean-Stark Distillate

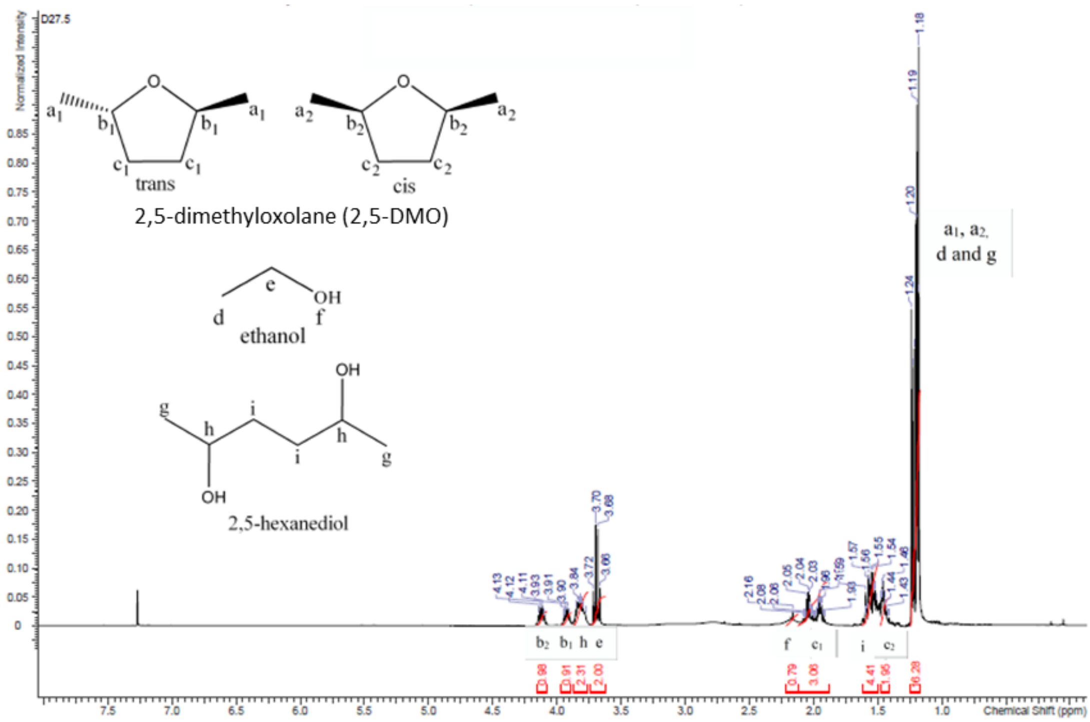

Figure S1. ^{1}H NMR spectrum of distillate collected in Dean-Stark trap during synthesis of 2,5-PHAF0.7. $CDCl_3$ solvent, 400 MHz.

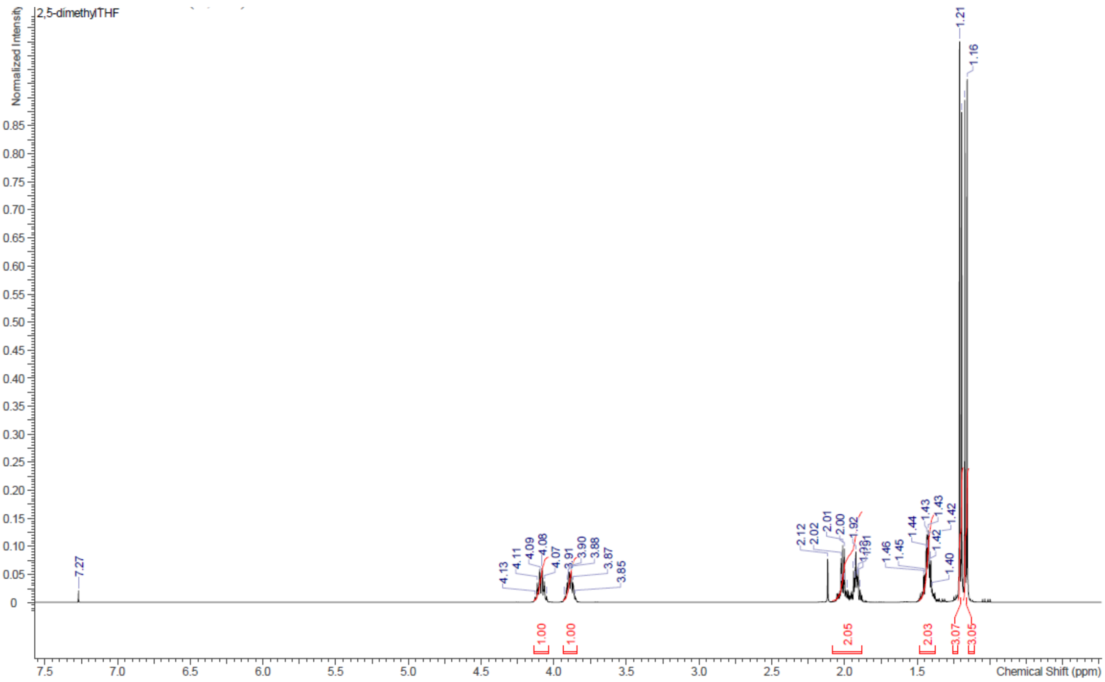

Figure S2. ^{1}H NMR spectrum of pure 2,5-dimethyloxolane (2,5-DMO) for comparative purposes to Figure S1. $CDCl_3$ solvent, 400 MHz.

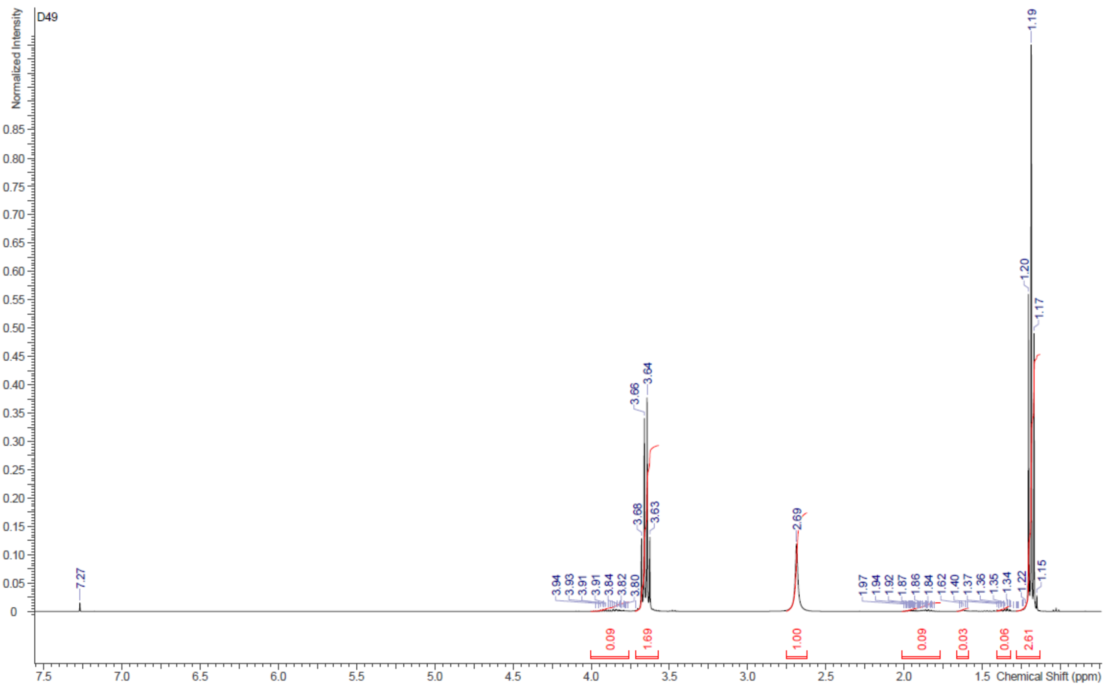

Figure S3. ^{1}H NMR spectrum of distillate collected in Dean-Stark trap during synthesis of 1,4-PPAF0.5. $CDCl_3$ solvent, 400 MHz. Small quantities of 2-methyl oxolane are present alongside ethanol and diol, as expected.

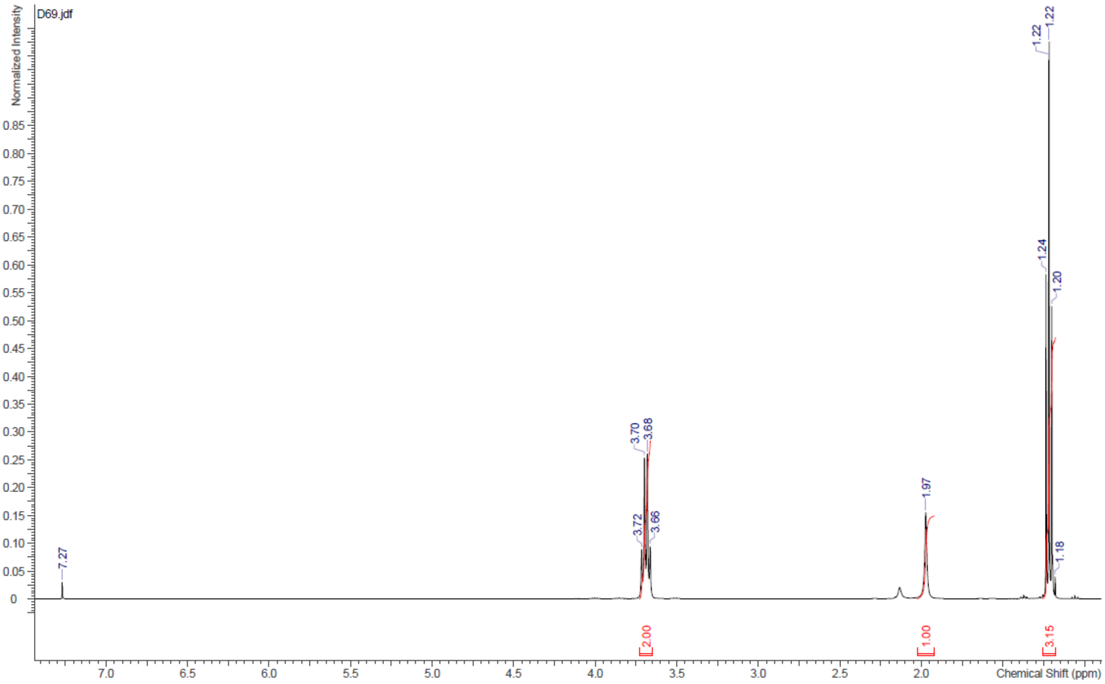

Figure S4. [1]H NMR spectrum of distillate collected in Dean-Stark trap during synthesis of 1,6-PHAF0.5. $CDCl_3$ solvent, 400 MHz. Essentially ethanol, as expected.

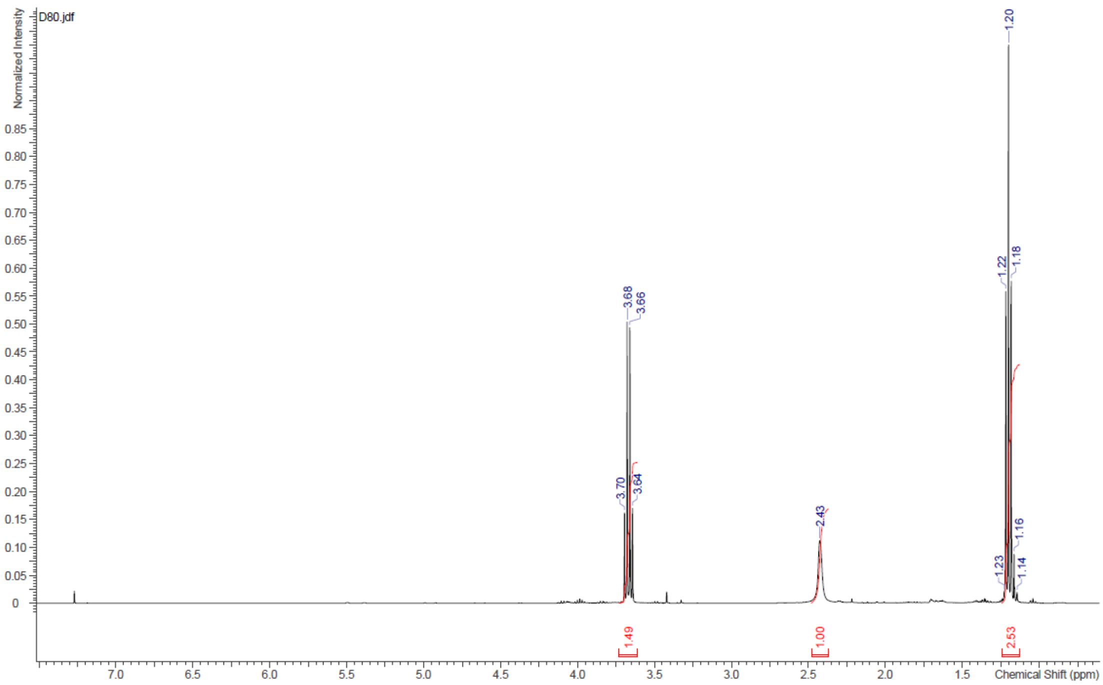

Figure S5. [1]H NMR spectrum of distillate collected in Dean-Stark trap during synthesis of 2,7-POAF0.6. $CDCl_3$ solvent, 400 MHz. Essentially ethanol and small quantities of diol (2,7-ODO), as expected.

S3. [1]H-NMR Spectra of Polyesters, Including End-Group Analysis

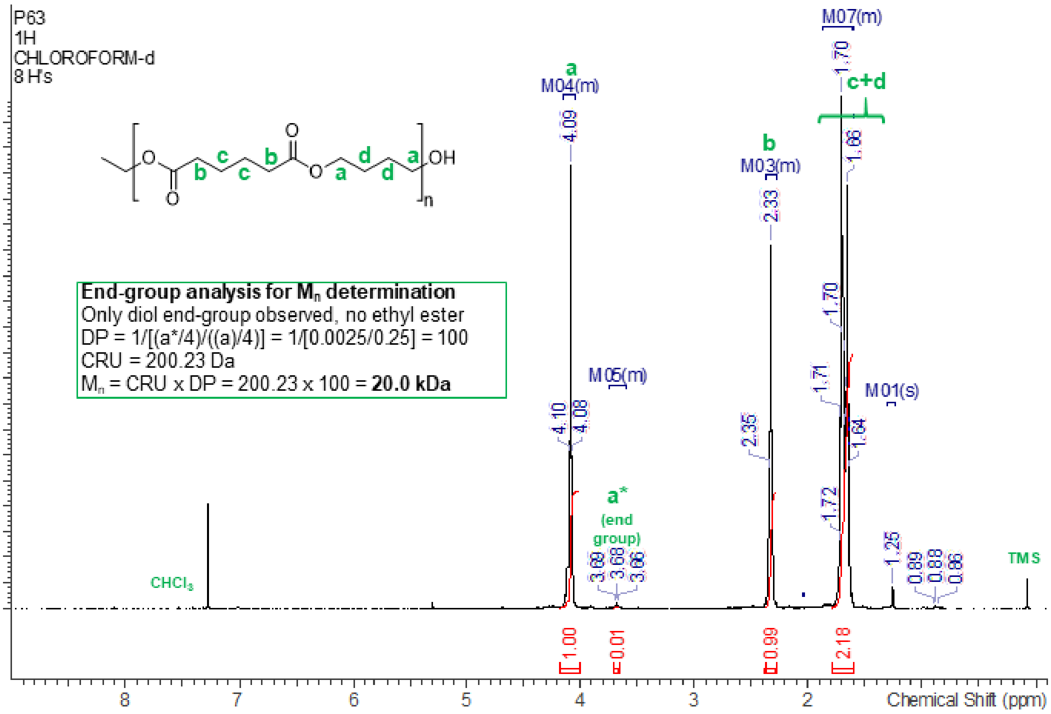

Figure S6. [1]H NMR Spectrum of 1,4-PBA. $CDCl_3$ solvent, 400 MHz, TMS standard.

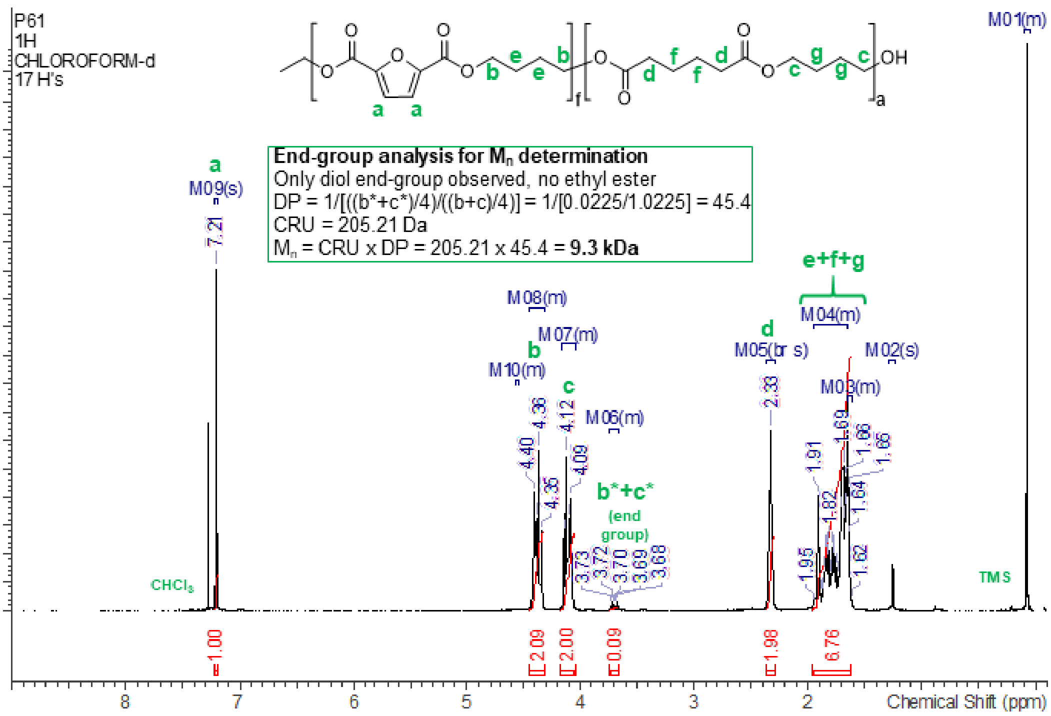

Figure S7. [1]H NMR Spectrum of 1,4-PBAF0.5. $CDCl_3$ solvent, 400 MHz, TMS standard.

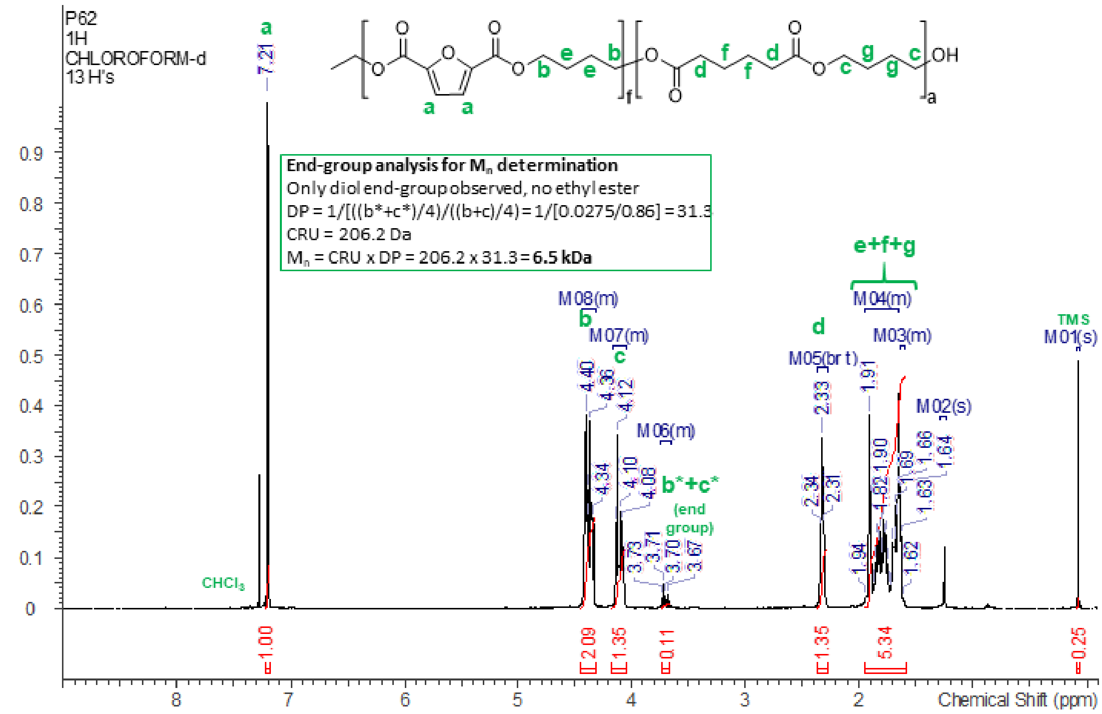

Figure S8. ^{1}H NMR Spectrum of 1,4-PBAF0.6. $CDCl_3$ solvent, 400 MHz, TMS standard.

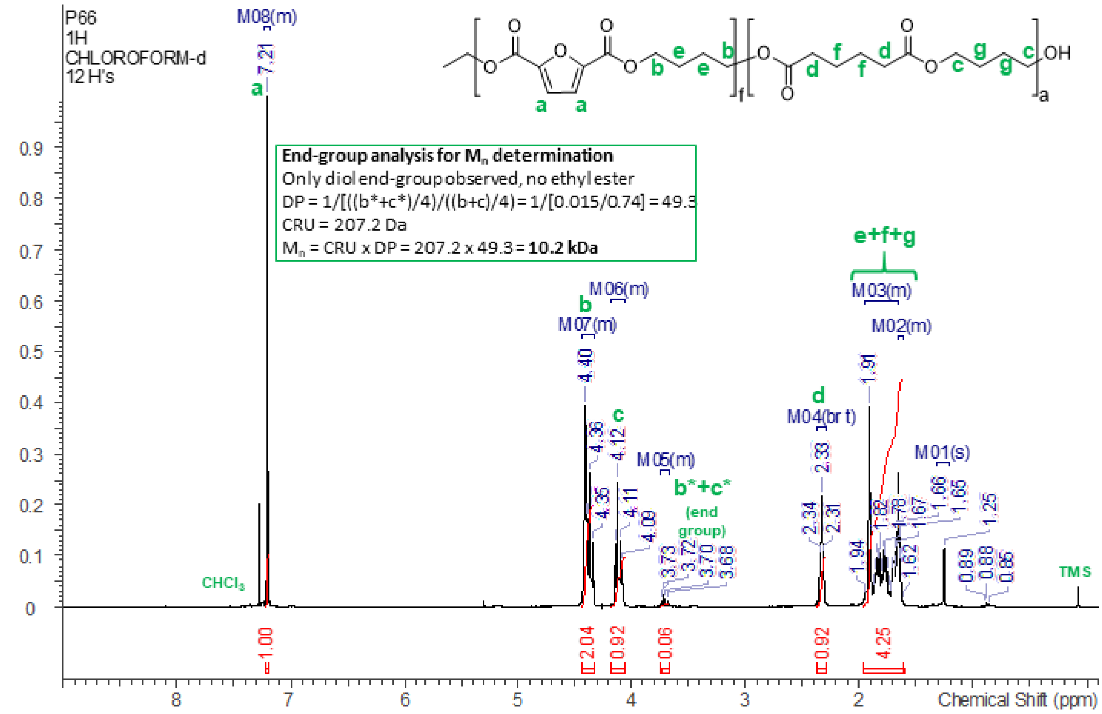

Figure S9. ^{1}H NMR Spectrum of 1,4-PBAF0.7. $CDCl_3$ solvent, 400 MHz, TMS standard.

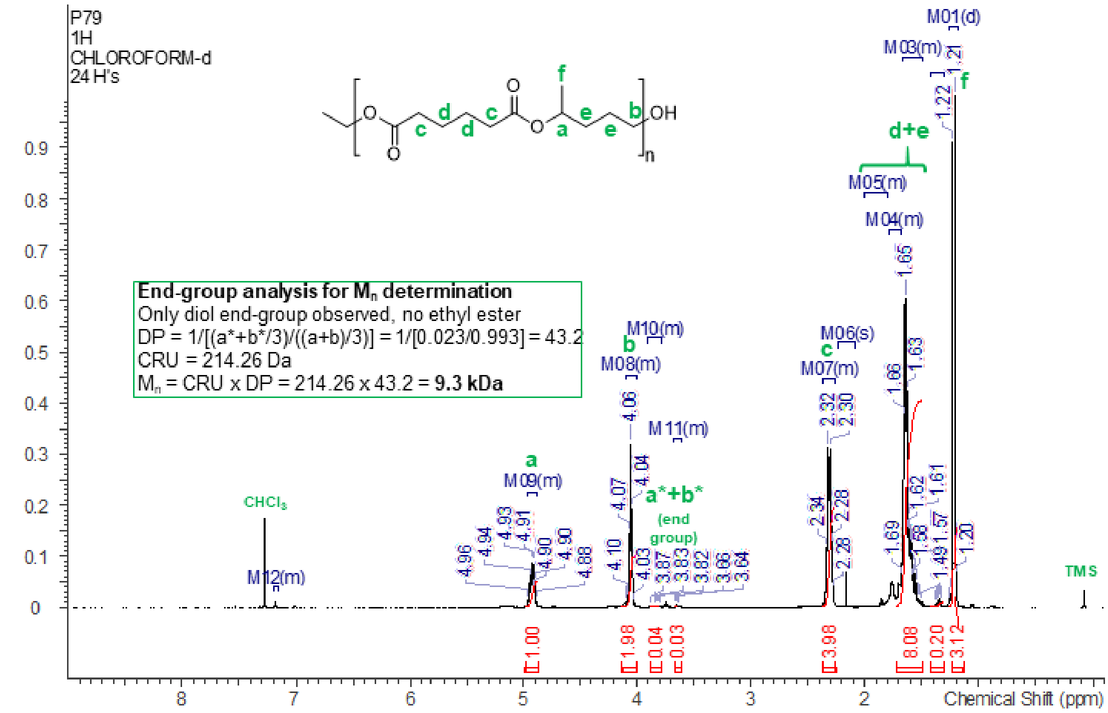

Figure S10. [1]H NMR Spectrum of 1,4-PPA. $CDCl_3$ solvent, 400 MHz, TMS standard.

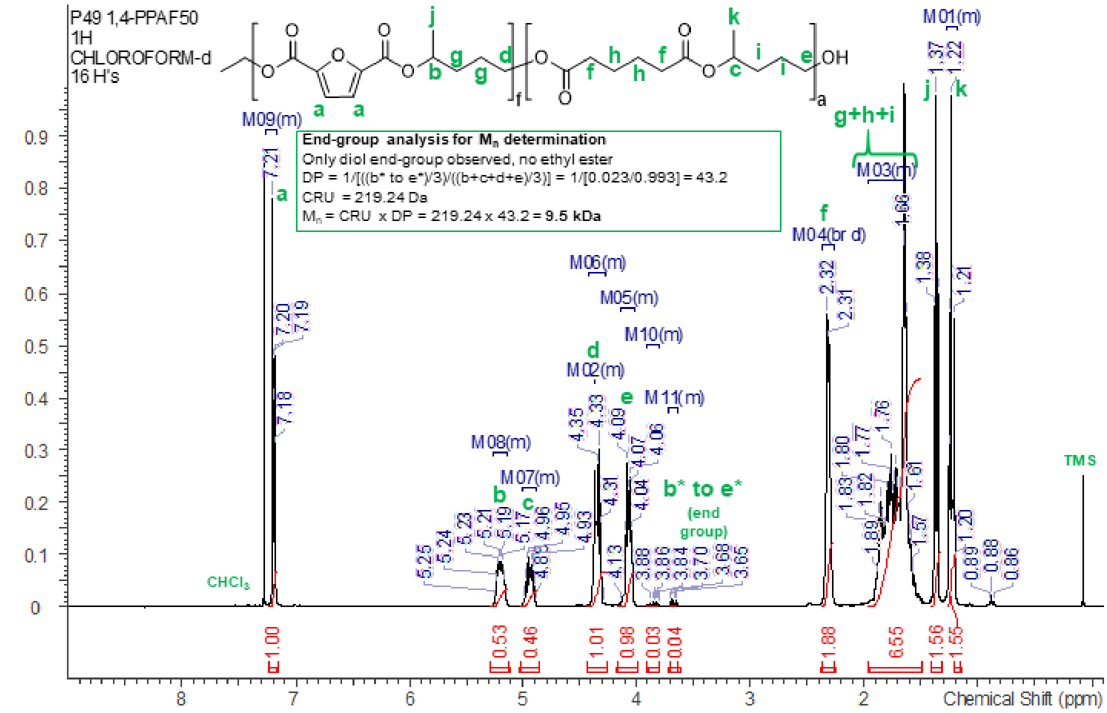

Figure S11. [1]H NMR Spectrum of 1,4-PPAF0.5. $CDCl_3$ solvent, 400 MHz, TMS standard.

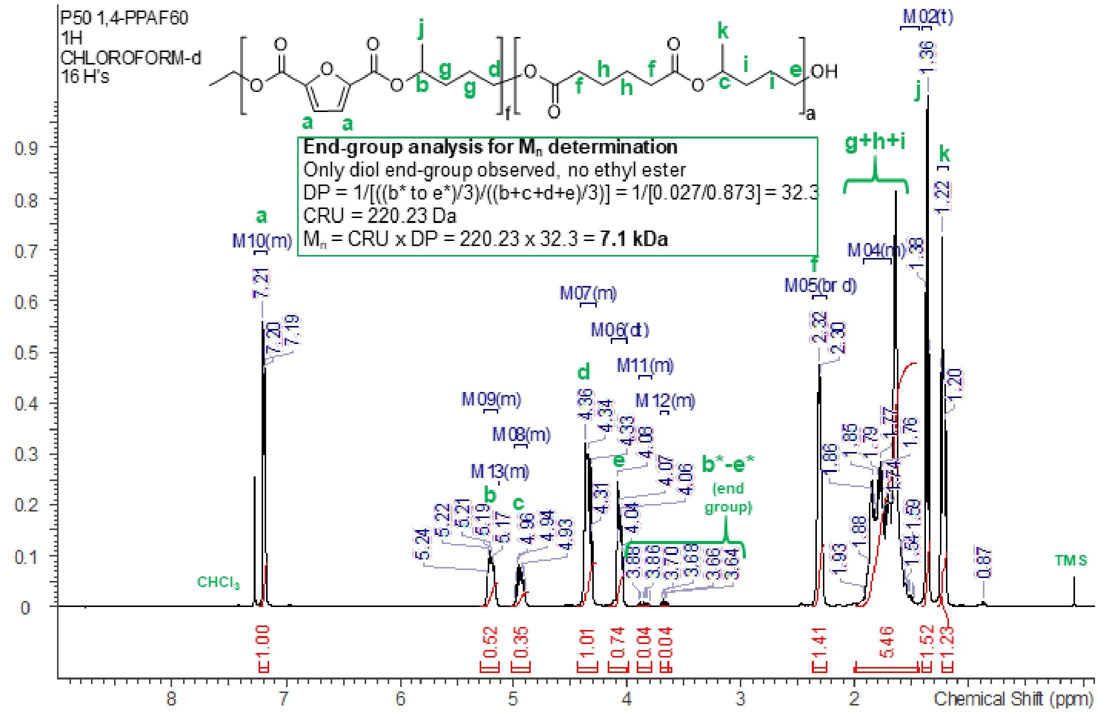

Figure S12. ^{1}H NMR Spectrum of 1,4-PPAF0.6. $CDCl_3$ solvent, 400 MHz, TMS standard.

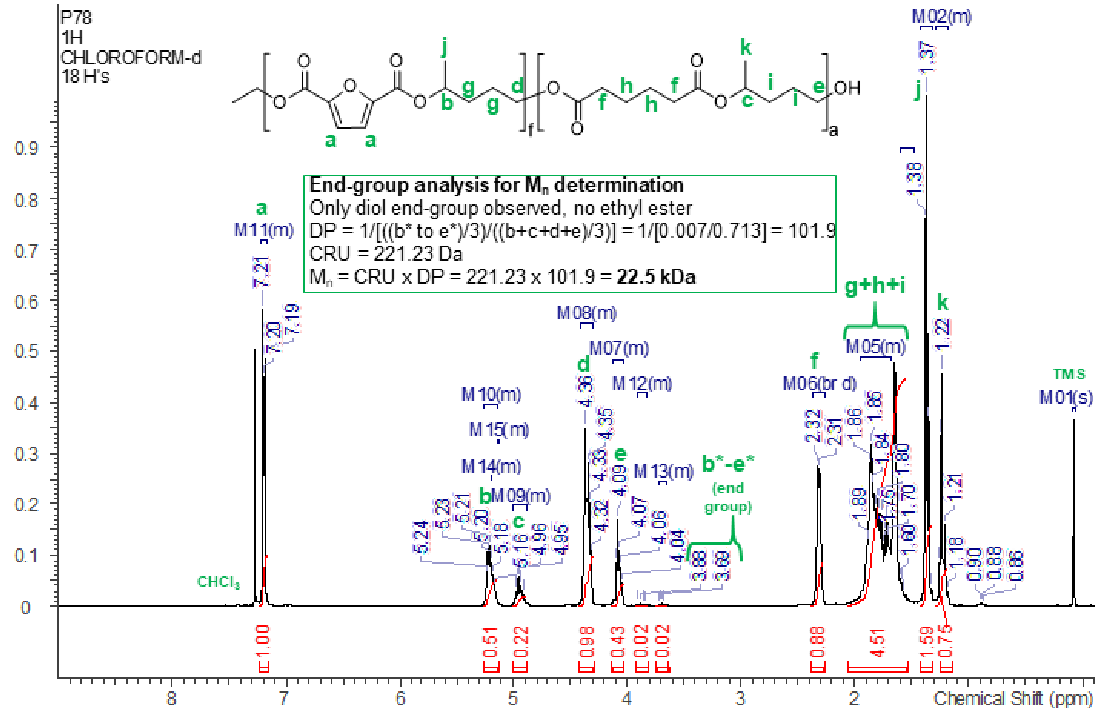

Figure S13. ^{1}H NMR Spectrum of 1,4-PPAF0.7. $CDCl_3$ solvent, 400 MHz, TMS standard.

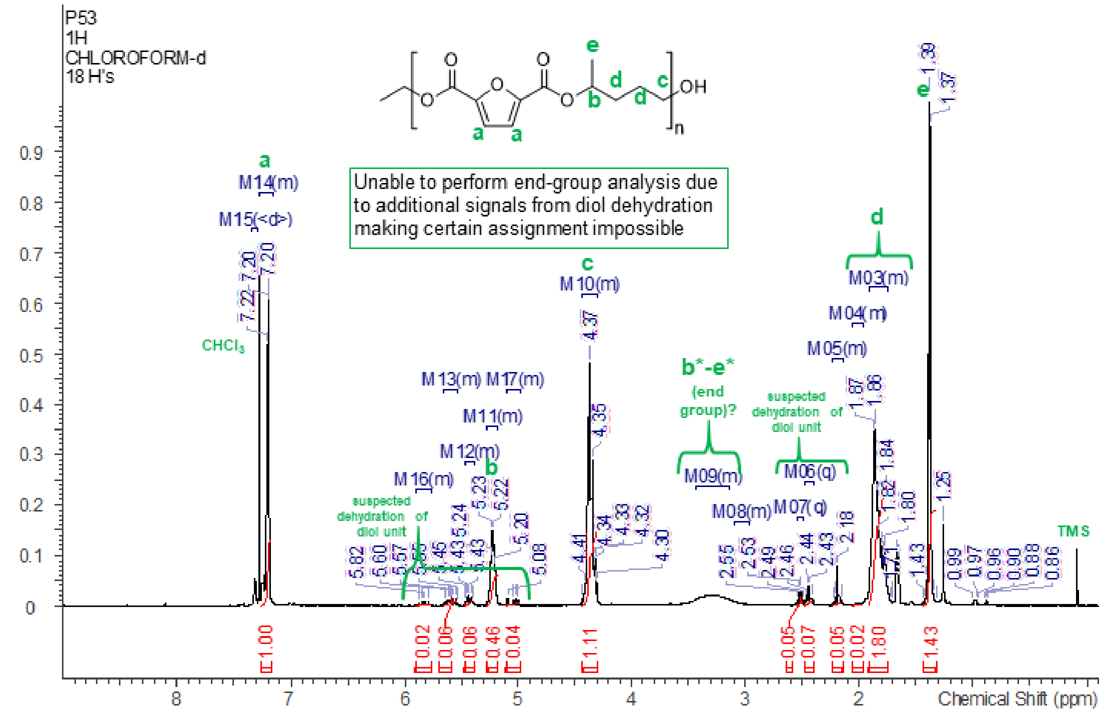

Figure S14. ^{1}H NMR Spectrum of 1,4-PPF. $CDCl_3$ solvent, 400 MHz, TMS standard.

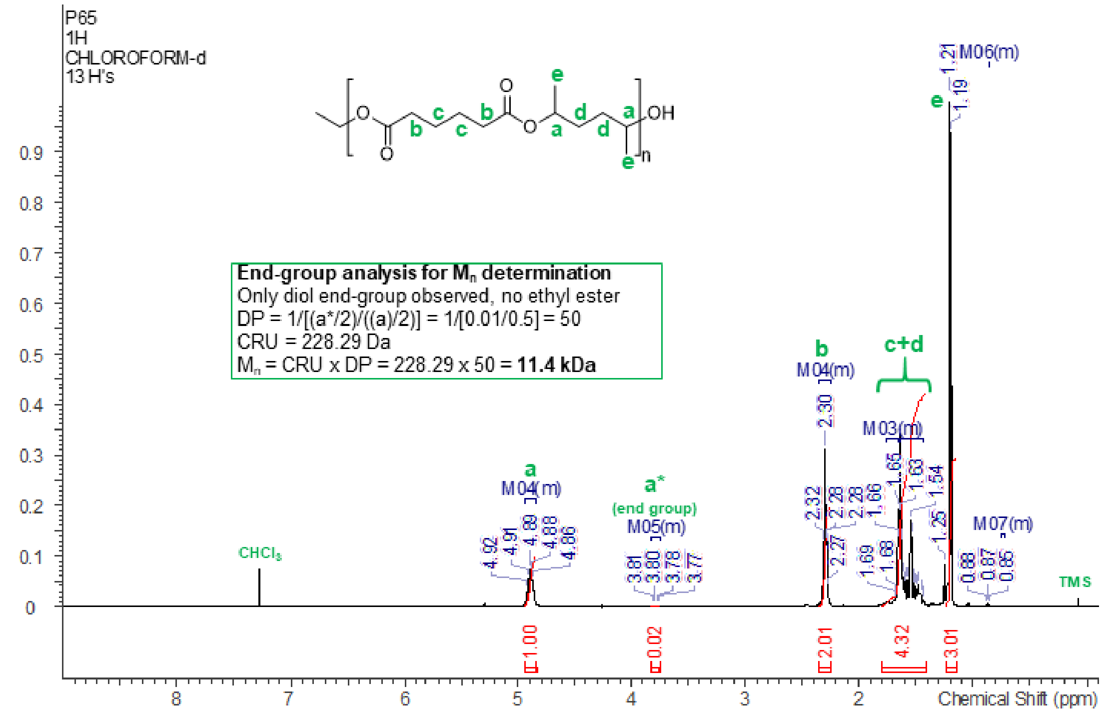

Figure S15. ^{1}H NMR Spectrum of 2,5-PHA. $CDCl_3$ solvent, 400 MHz, TMS standard.

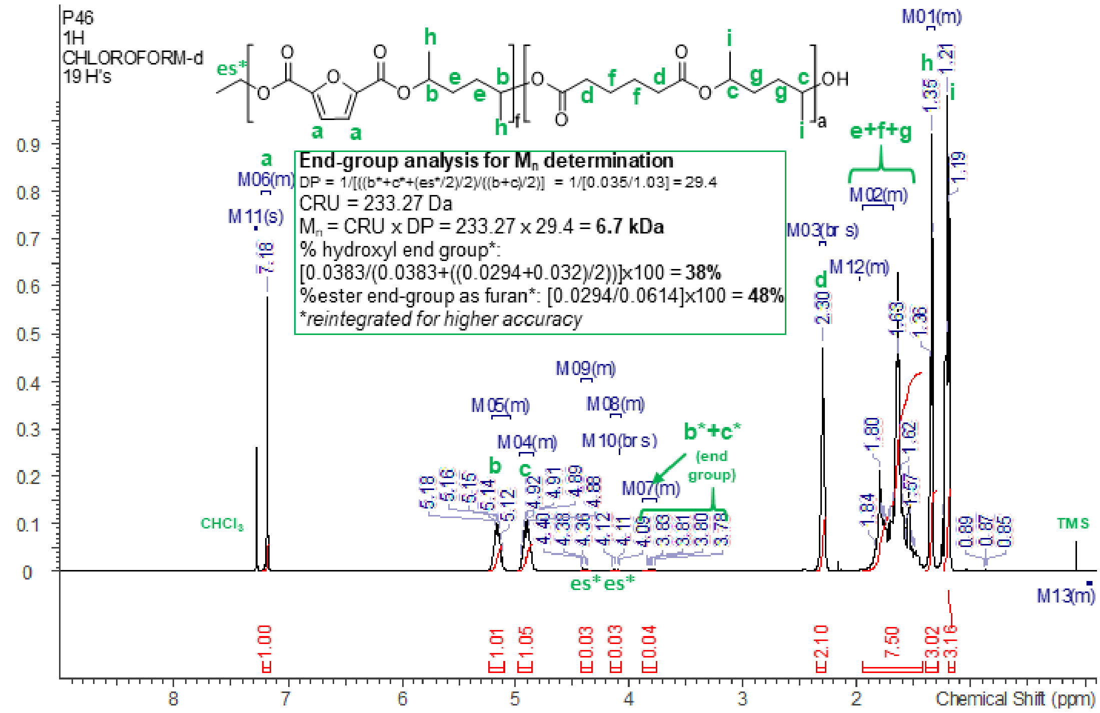

Figure S16. ^{1}H NMR Spectrum of 2,5-PHAF0.5. $CDCl_3$ solvent, 400 MHz, TMS standard.

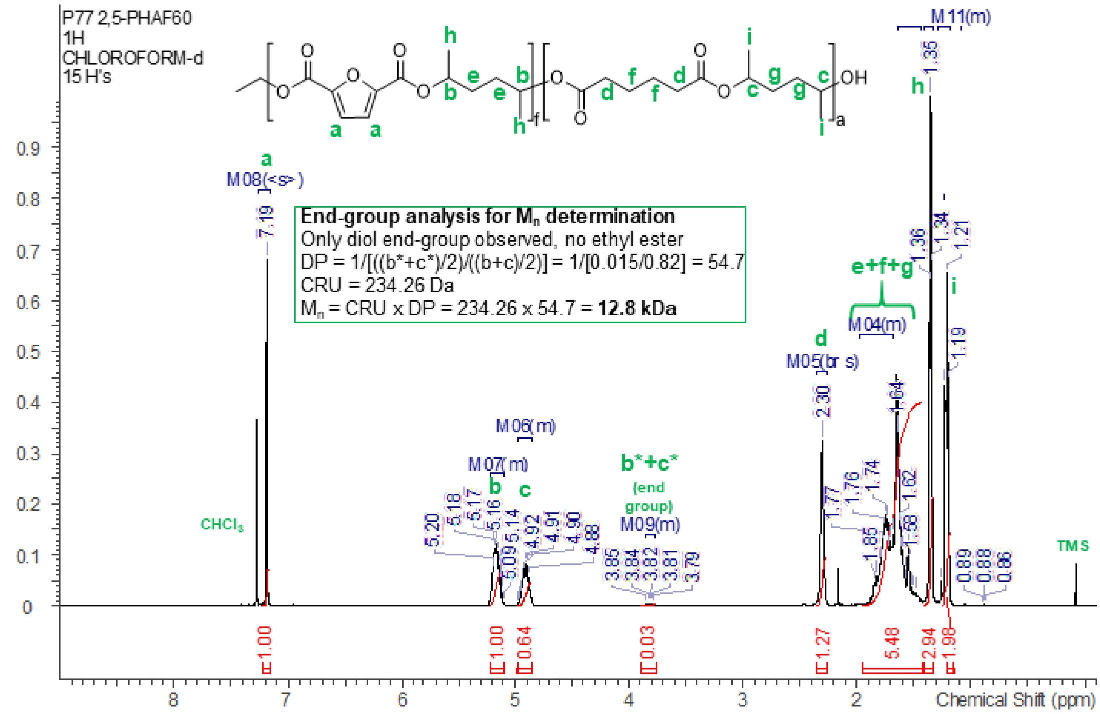

Figure S17. ^{1}H NMR Spectrum of 2,5-PHAF0.6. $CDCl_3$ solvent, 400 MHz, TMS standard.

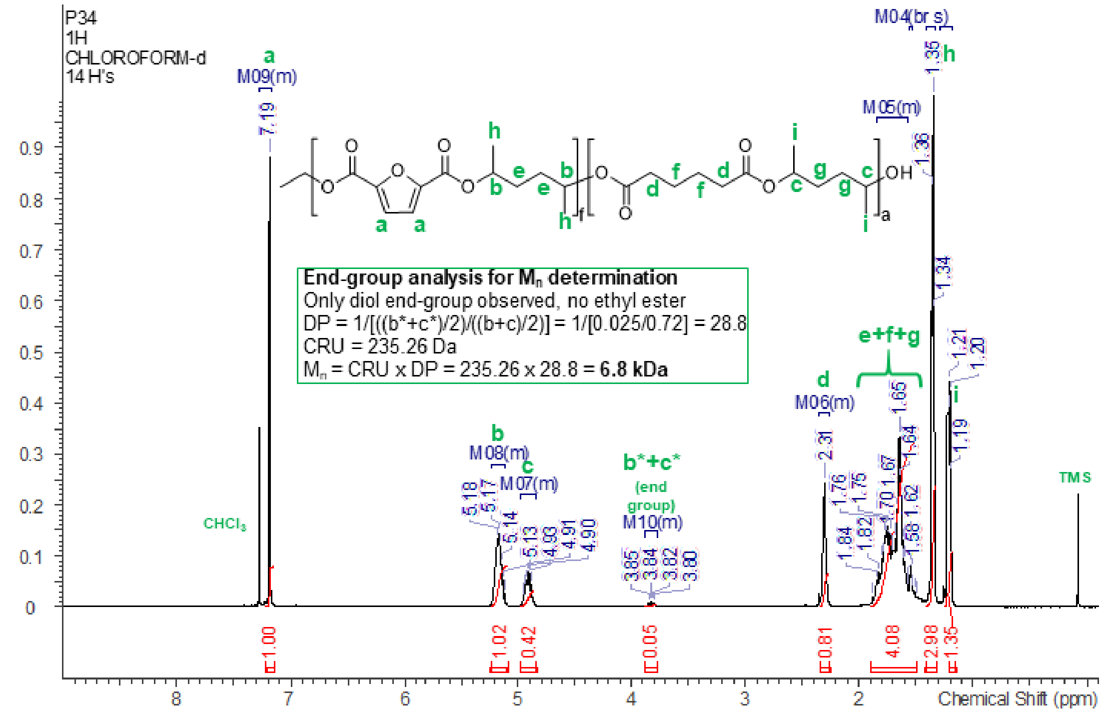

Figure S18. ^{1}H NMR Spectrum of 2,5-PHAF0.7. $CDCl_3$ solvent, 400 MHz, TMS standard.

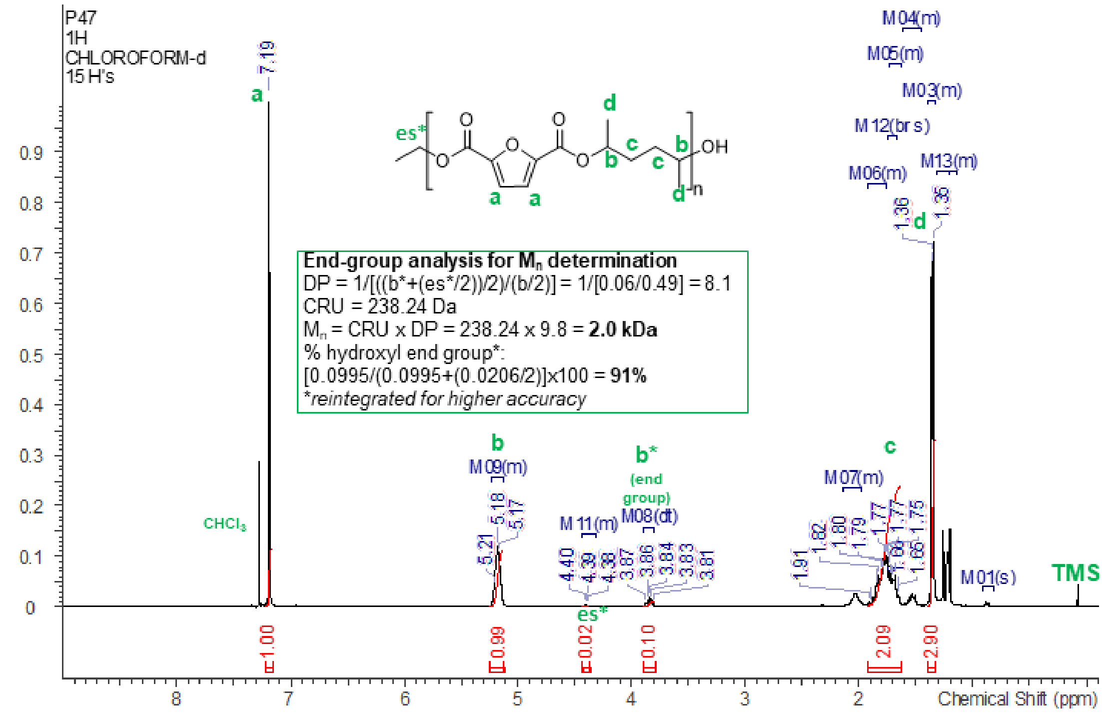

Figure S19. ^{1}H NMR Spectrum of 2,5-PHF. $CDCl_3$ solvent, 400 MHz, TMS standard.

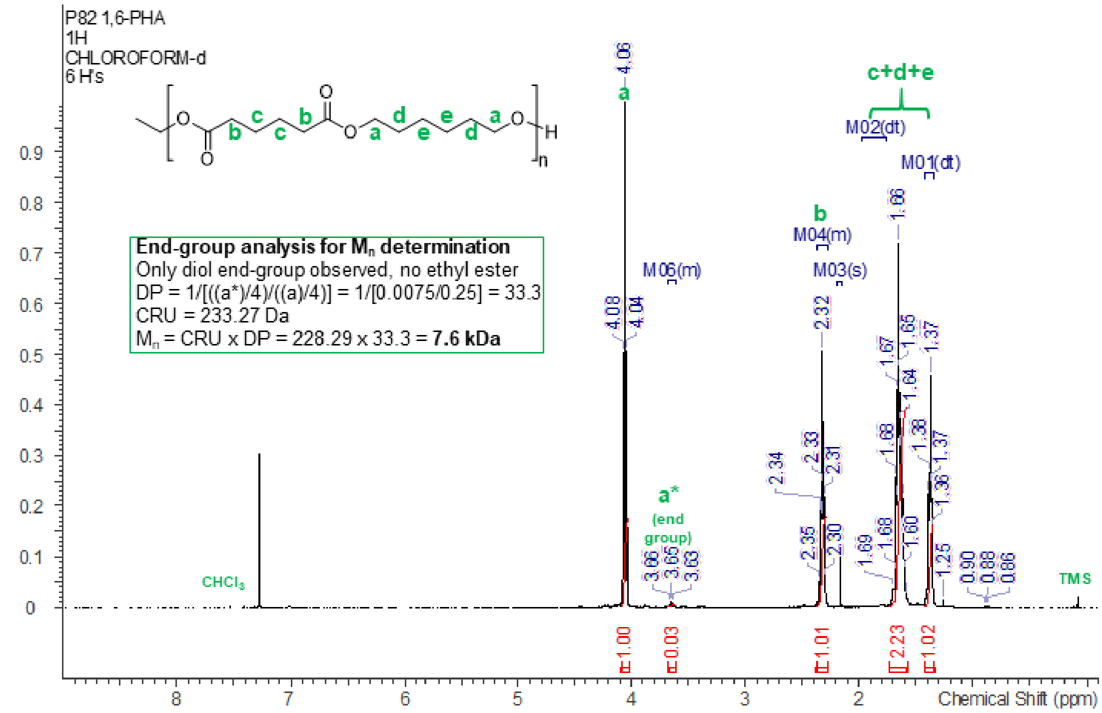

Figure S20. ^{1}H NMR Spectrum of 1,6-PHA. $CDCl_3$ solvent, 400 MHz, TMS standard.

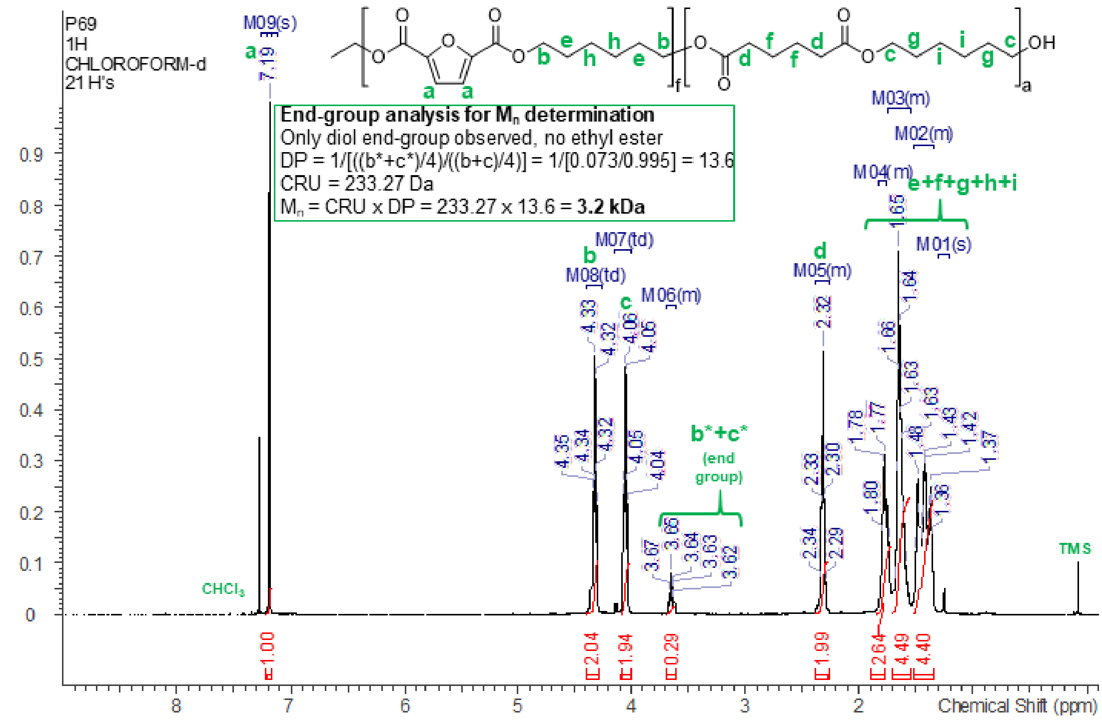

Figure S21. ^{1}H NMR Spectrum of 1,6-PHAF0.5. $CDCl_3$ solvent, 400 MHz, TMS standard.

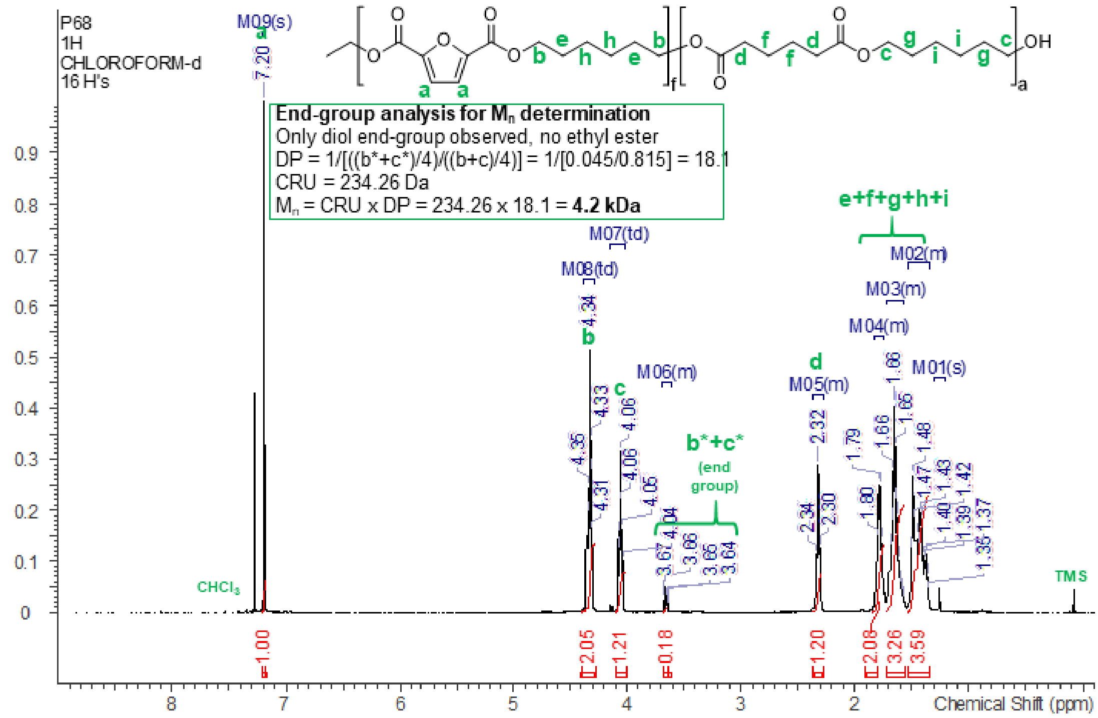

Figure S22. [1]H NMR Spectrum of 1,6-PHAF0.6. $CDCl_3$ solvent, 400 MHz, TMS standard.

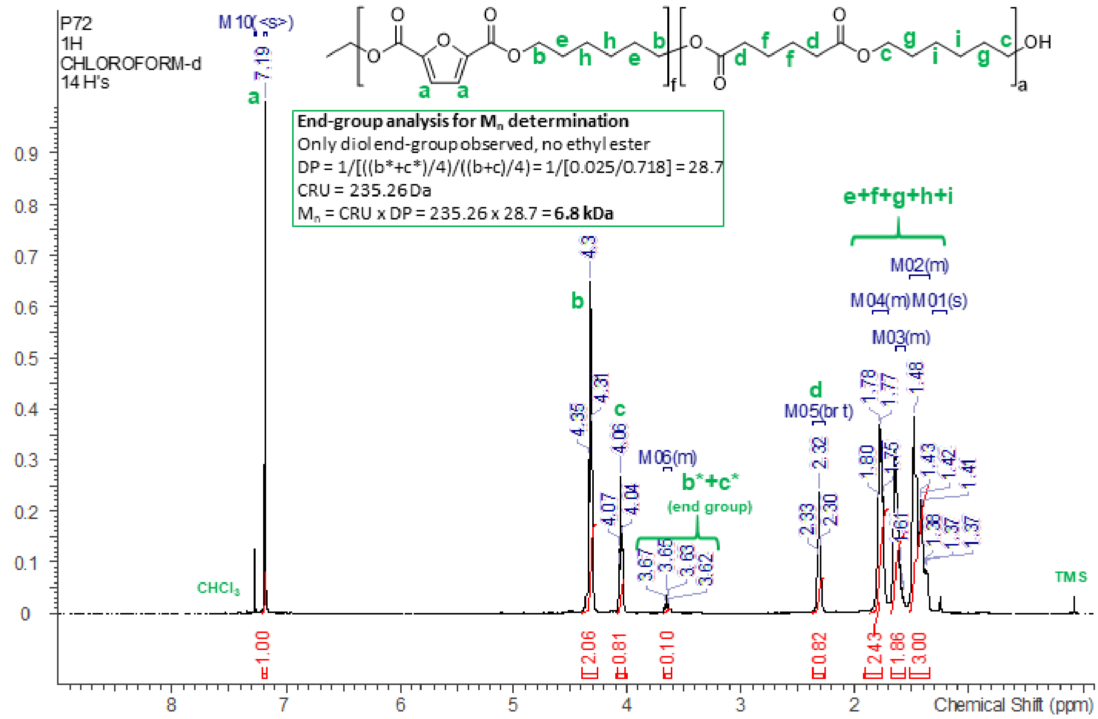

Figure S23. [1]H NMR Spectrum of 1,6-PHAF0.7. $CDCl_3$ solvent, 400 MHz, TMS standard.

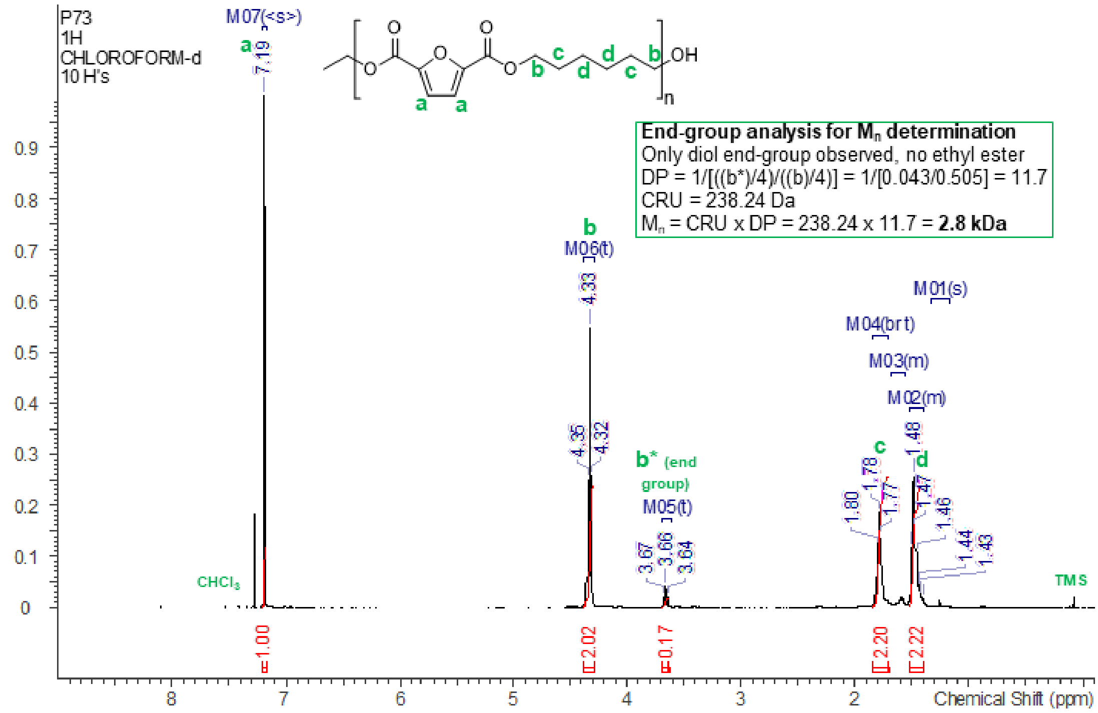

Figure S24. [1]H NMR Spectrum of 1,6-PHF. $CDCl_3$ solvent, 400 MHz, TMS standard.

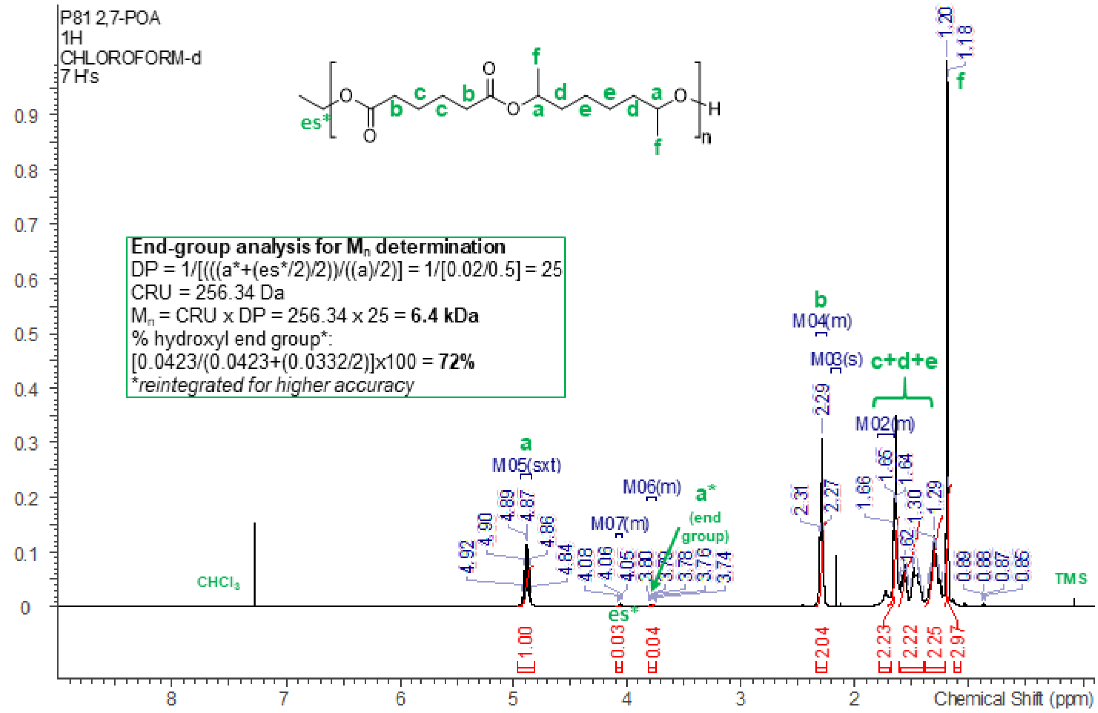

Figure S25. [1]H NMR Spectrum of 2,7-POA. $CDCl_3$ solvent, 400 MHz, TMS standard.

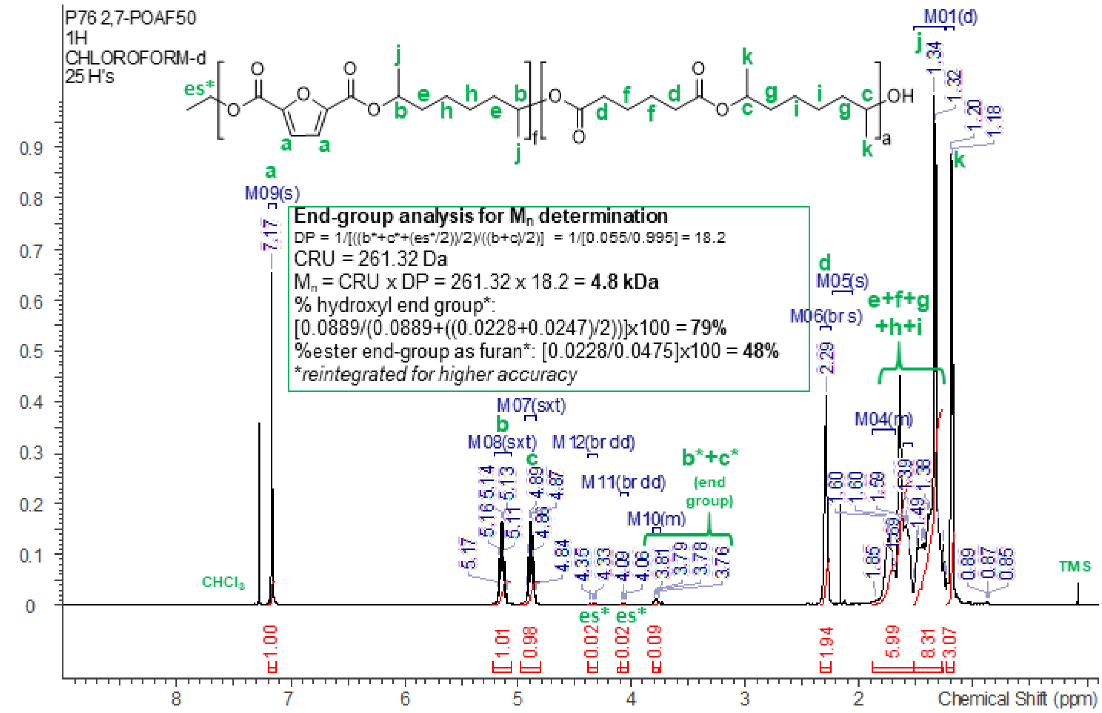

Figure S26. [1]H NMR Spectrum of 2,7-POAF0.5. $CDCl_3$ solvent, 400 MHz, TMS standard.

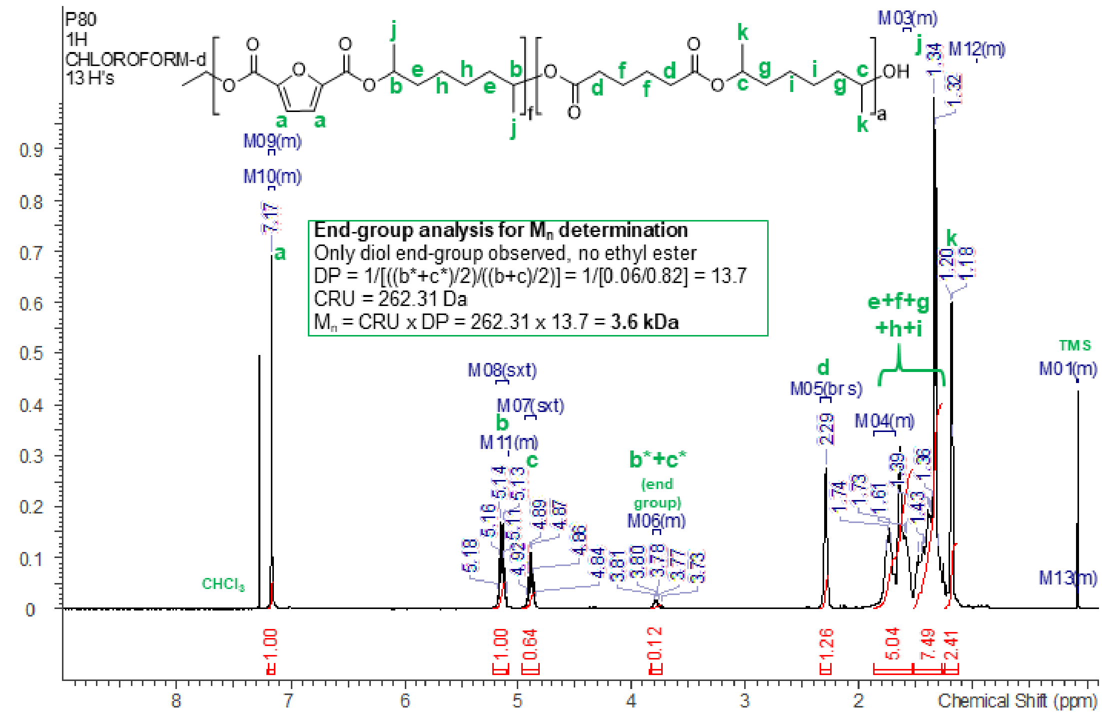

Figure S27. [1]H NMR Spectrum of 2,7-POAF0.6. $CDCl_3$ solvent, 400 MHz, TMS standard.

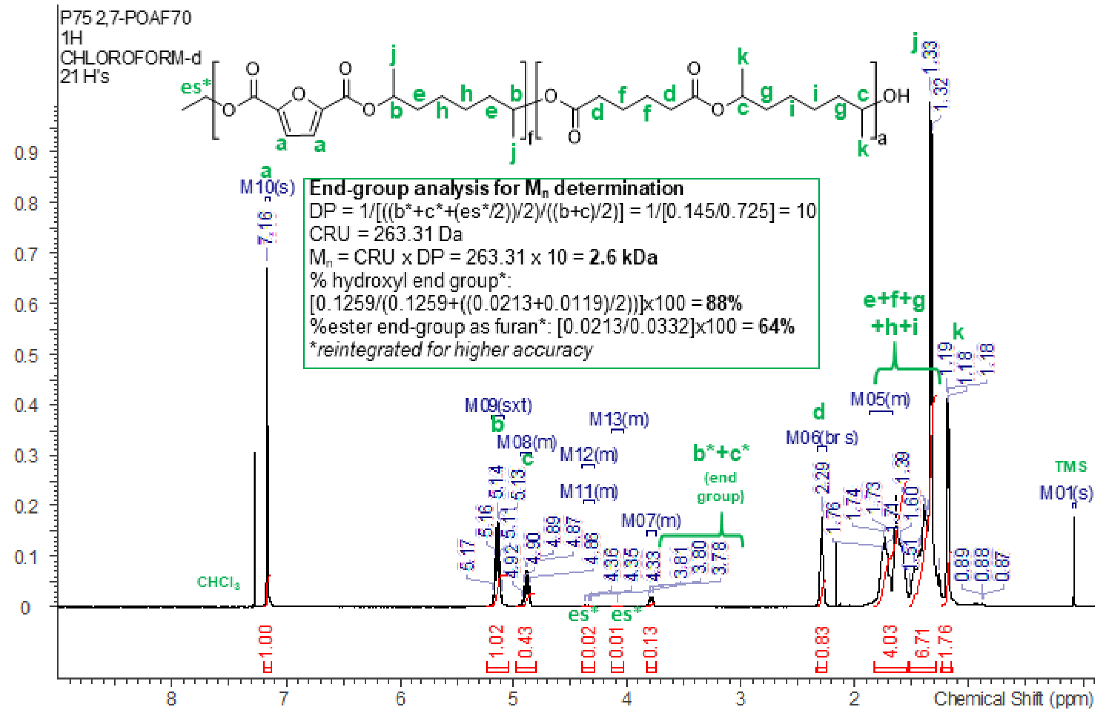

Figure S28. [1]H NMR Spectrum of 2,7-POAF0.7. $CDCl_3$ solvent, 400 MHz, TMS standard.

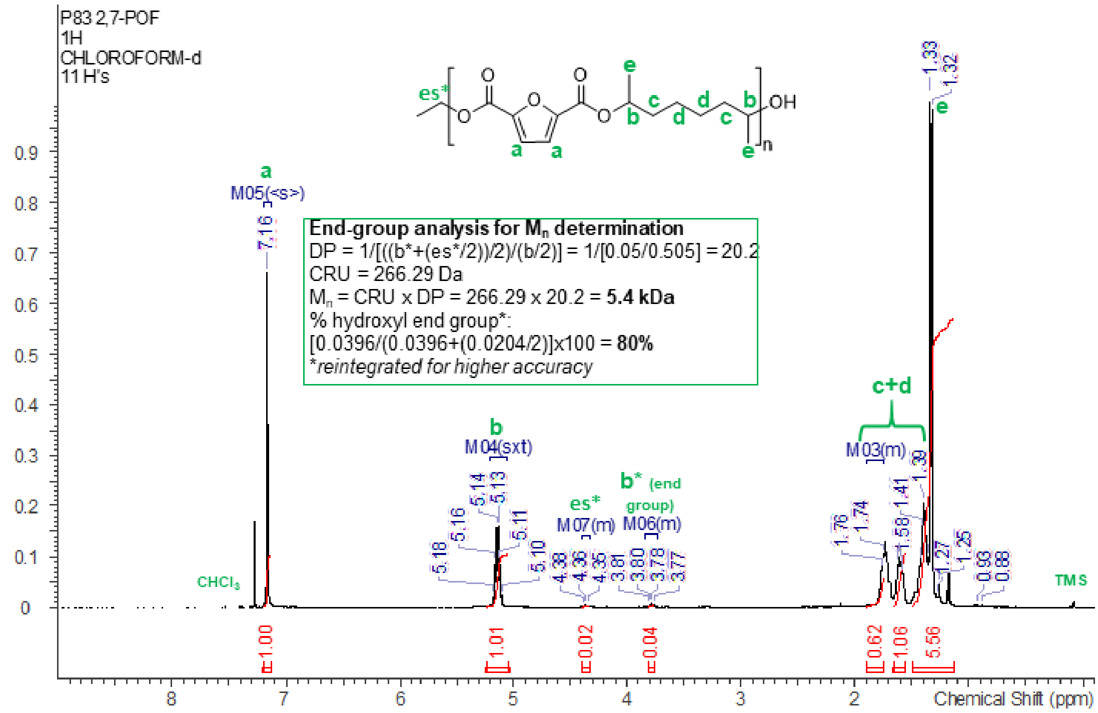

Figure S29. [1]H NMR Spectrum of 2,7-POF. $CDCl_3$ solvent, 400 MHz, TMS standard.

S4. Chromatograms from GPC Analysis of Copolyesters

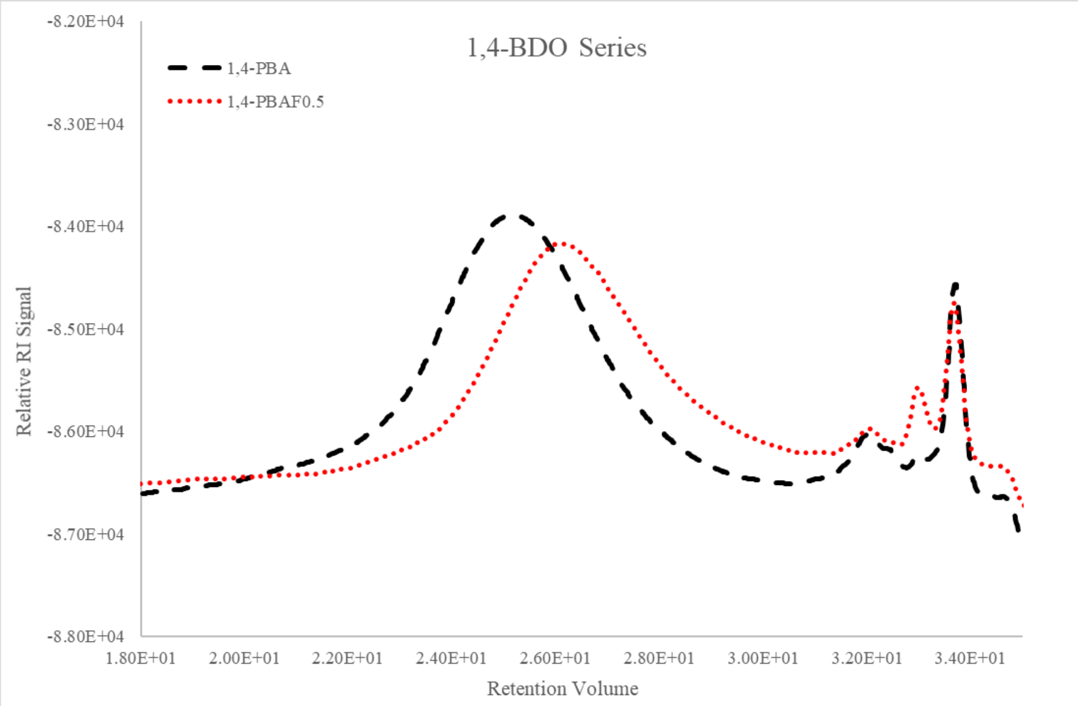

Figure S30. Overlayed GPC chromatograms for the 1,4-BDO series of polyesters. Experimental details in main manuscript. Raw eluogram data and mass distribution available via the data access statement in the main manuscript.

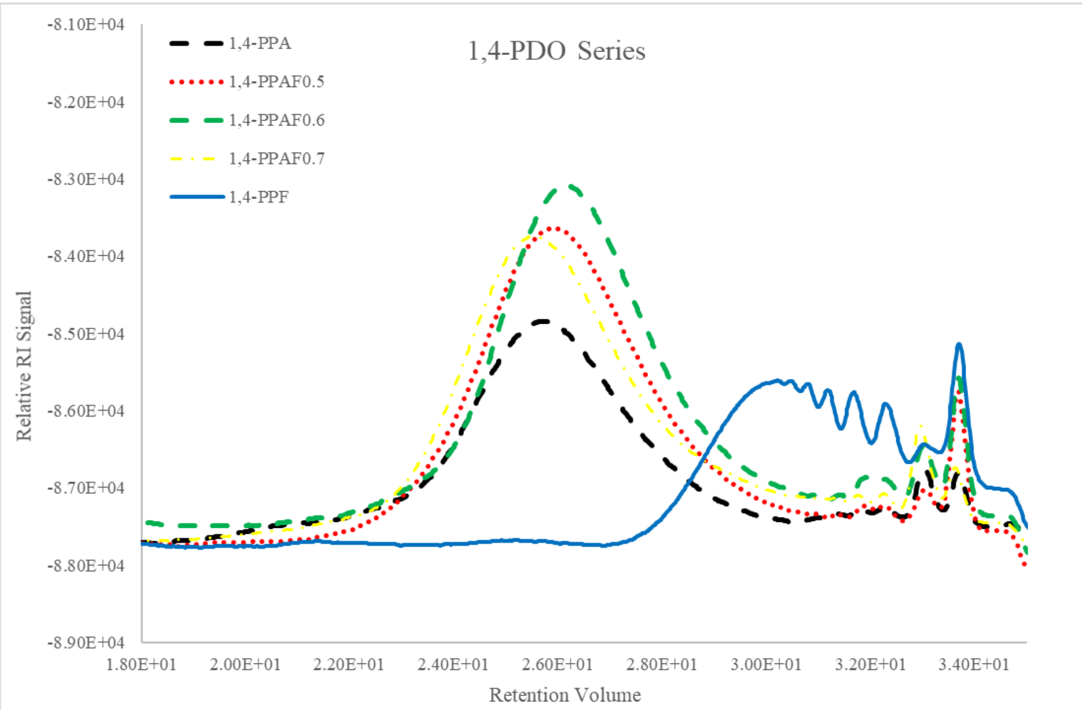

Figure S31. Overlayed GPC chromatograms for the 1,4-PDO series of polyesters. Experimental details in main manuscript. Raw eluogram data and mass distribution available via the data access statement in the main manuscript.

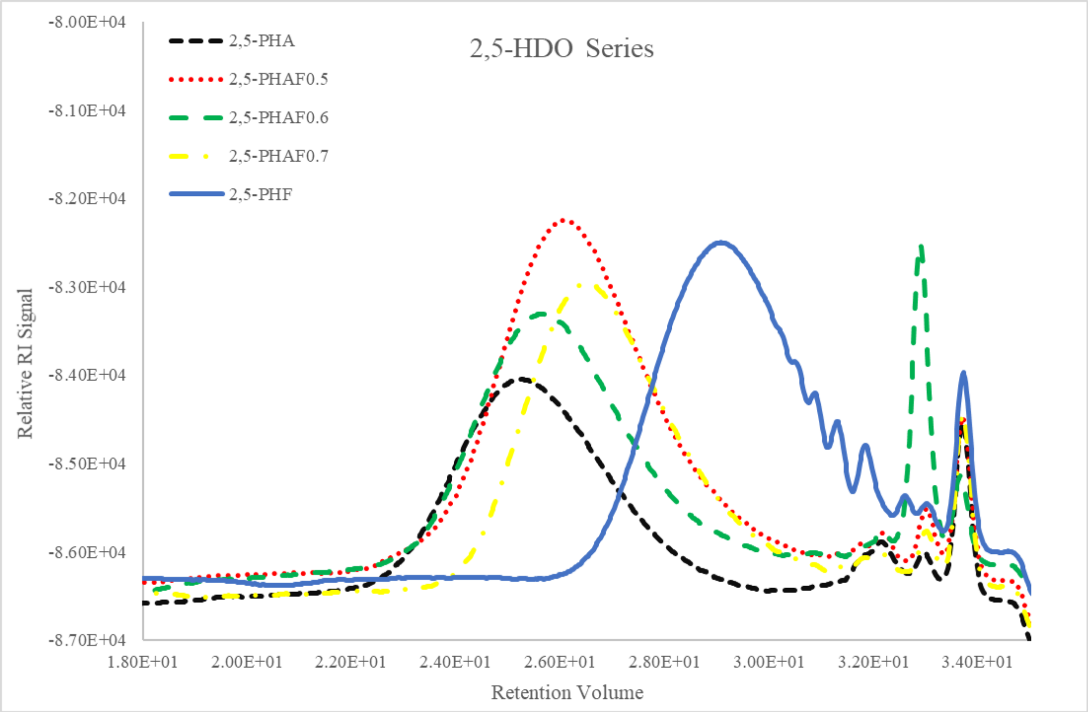

Figure S32. Overlayed GPC chromatograms for the 2,5-HDO series of polyesters. Experimental details in main manuscript. Raw eluogram data and mass distribution available via the data access statement in the main manuscript.

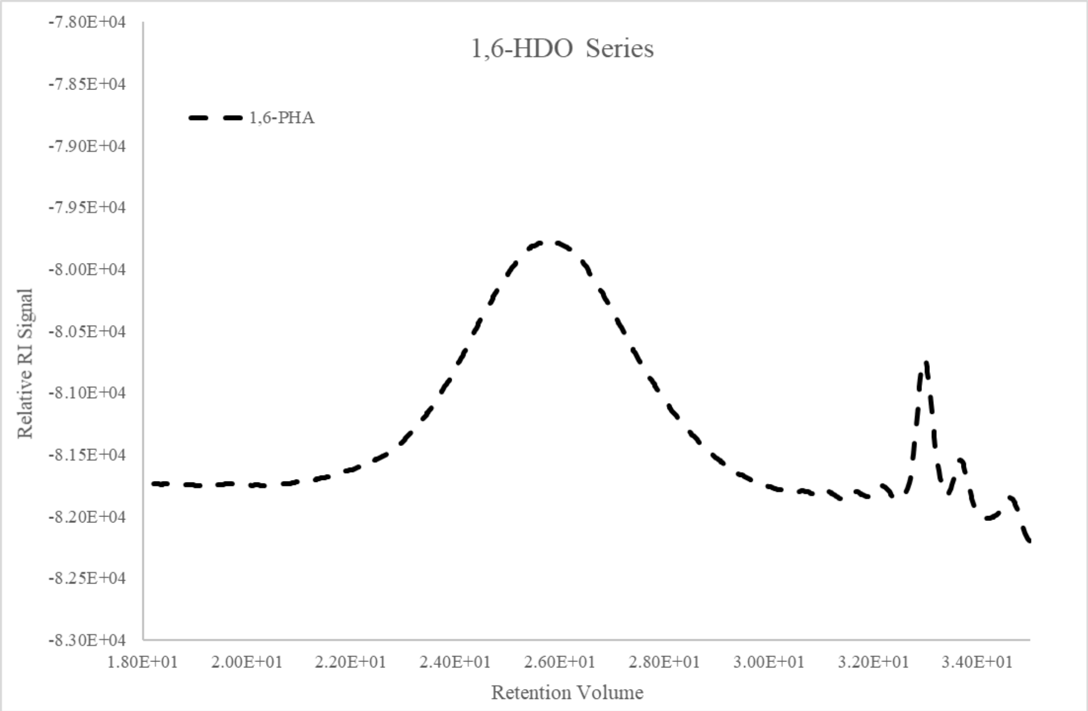

Figure S33. GPC chromatogram for 1,6-PHA. Experimental details in main manuscript. Raw eluogram data and mass distribution available via the data access statement in the main manuscript.

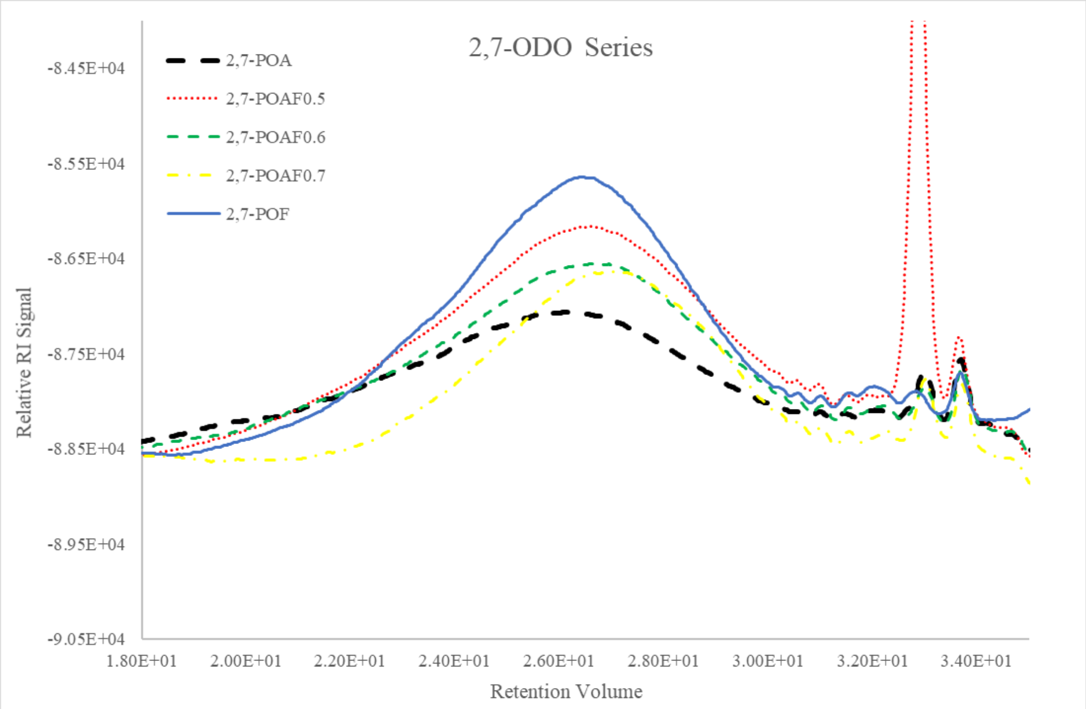

Figure S34. Overlayed GPC chromatograms for the 2,7-ODO series of polyesters. Experimental details in main manuscript. Raw eluogram data and mass distribution available via the data access statement in the main manuscript.

S5. Literature Values for GPC and DSC Analysis of Known Polyesters

Table S8. Literature values of equivalent polyesters where available.

Polymer	M_n / kDa	M_w / kDa	Đ	T_g / ˚C	T_m / ˚C	Reference
1,4-PBA	45	67	1.5	-62	67	Wu[4]
1,4-PBAF0.5	48	93	2	-20	70	Wu[4]
1,4-PBAF0.6	43	96	2.3	-11	112	Wu[4]
1,4-PBAF0.7	35	68	1.9	0	132	Wu[4]
1,4-PBF	-	-	-	36	168	Wu[4]
1,4-PPA	4.2	19	4.6	-52	-	van der Klis[5]
1,4-PPF	8.1	30	3.6	47	-	van der Klis[5]
2,5-PHA	5.5	20	3.6	-39	-	van der Klis[5]
2,5-PHA	8.9	15	1.7	-36	-	Arnaud[6]
2,5-PHAF0.5	11	16	1.5	2	-	Arnaud[6]
2,5-PHF	3.3	5.5	1.7	32	-	Arnaud[6]
2,5-PHF	5.7	14	2.4	51	-	van der Klis[5]
1,6-PHA	-	37	-59	58	-	Rohindra[7]
1,6-PHF	14	41	2.9	8	145	Haernvall[8]
2,7-POA	18	38	2.1	-44	-	Arnaud[6]
2,7-POAF0.5	9.9	19	2	-8	-	Arnaud[6]
2,7-POF	6.4	9.9	1.6	34	-	Arnaud[6]

S6. DSC Analysis of Copolyesters

All DSC analysis involved two heating cycles, below only the 2nd heating cycle is shown, T_g and T_m determined from these cycles. Full DSC results, including initial and first cycles and full data range, is given in the raw data files as mentioned in the main manuscript.

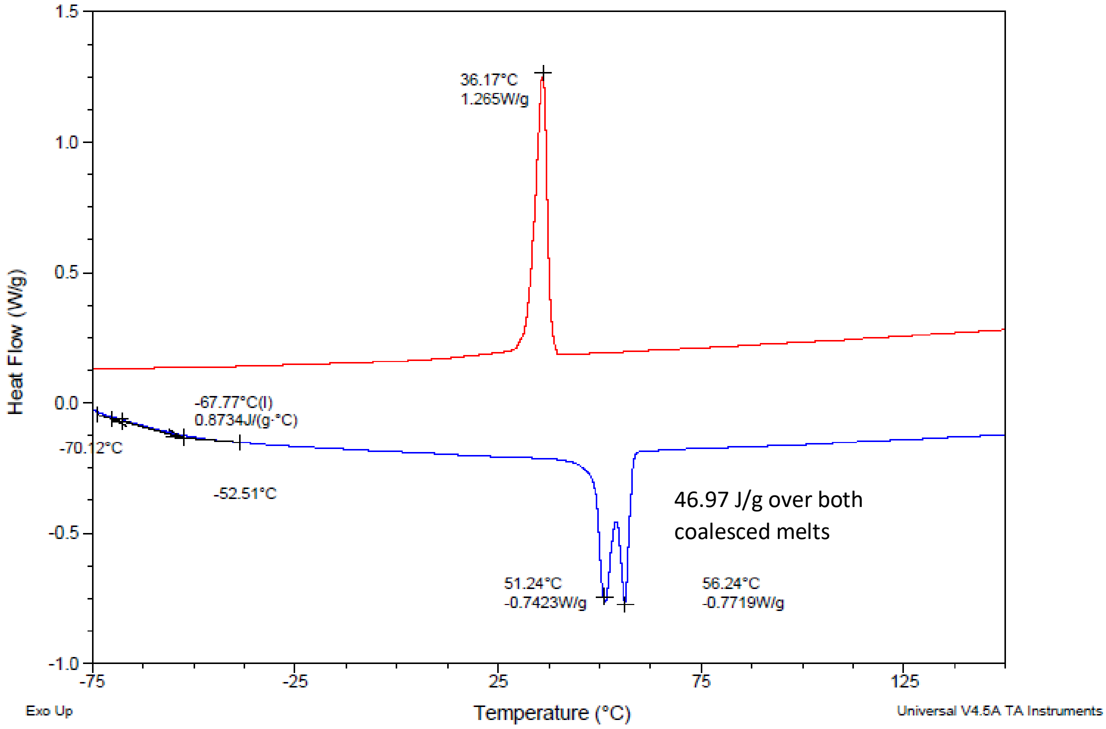

Figure S35. DSC Trace of 1,4-PBA. Experimental details in main manuscript. Displaying second heating cycle only, T_g and T_m determined from second heating cycle.

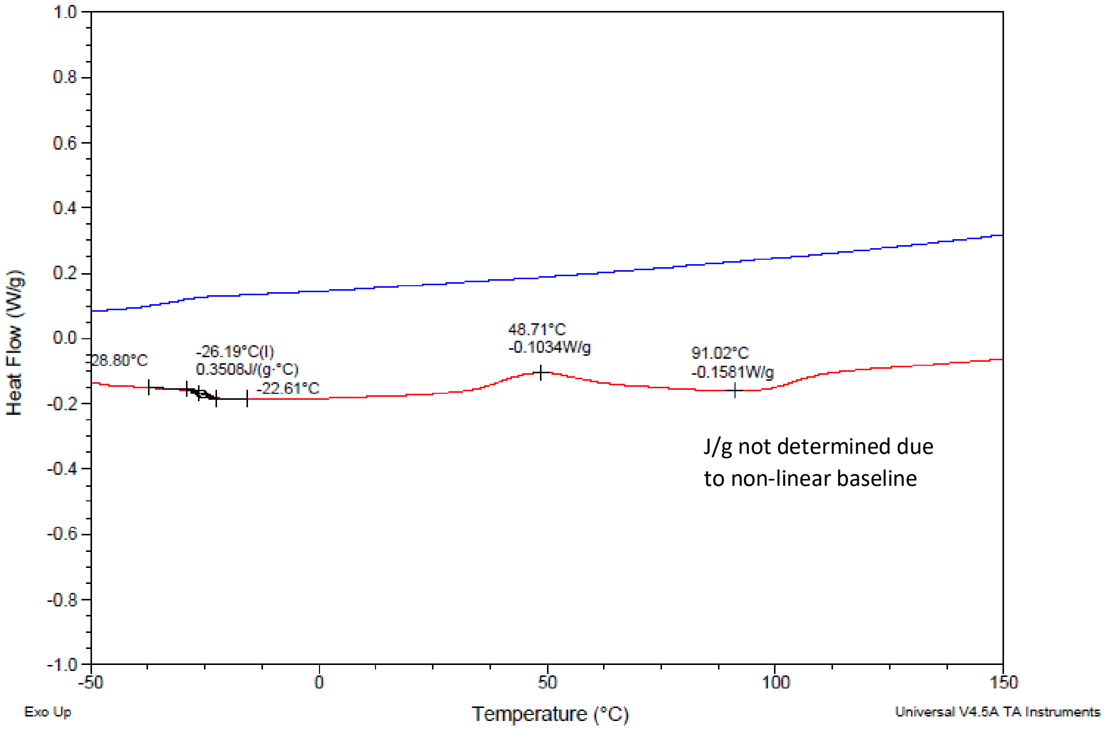

Figure S36. DSC Trace of 1,4-PBAF0.5. Experimental details in main manuscript. Displaying second heating cycle only, T_g and T_m determined from second heating cycle.

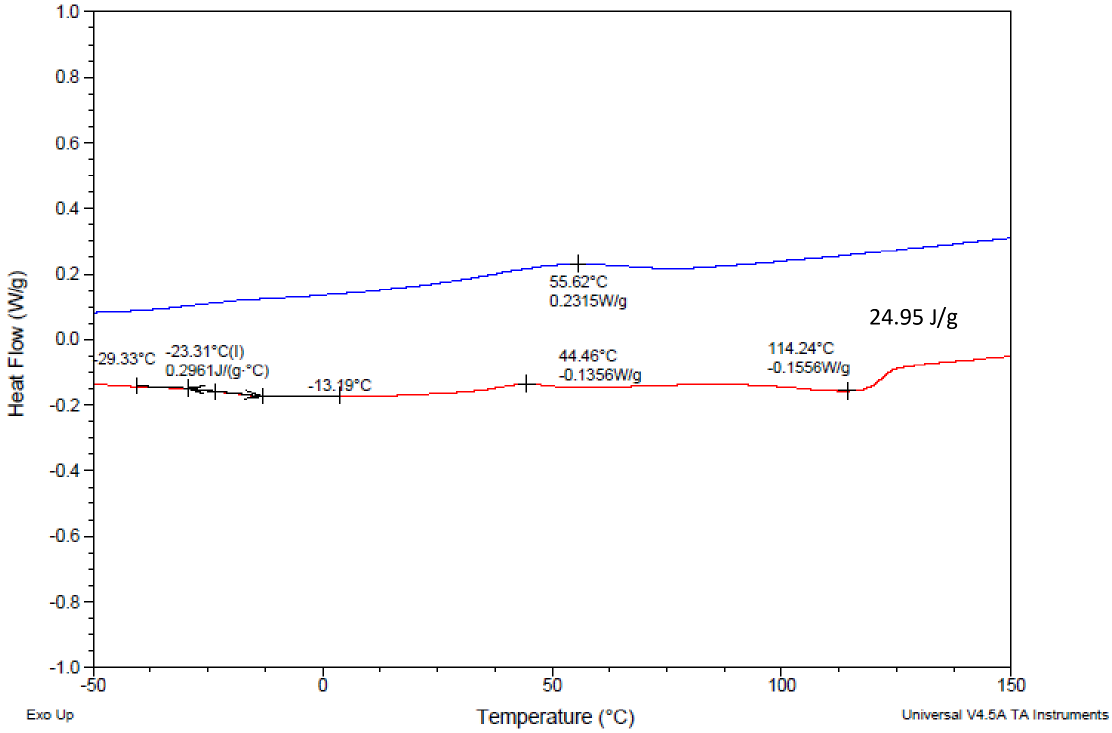

Figure S37. DSC Trace of 1,4-PBAF0.6. Experimental details in main manuscript. Displaying second heating cycle only, T_g and T_m determined from second heating cycle.

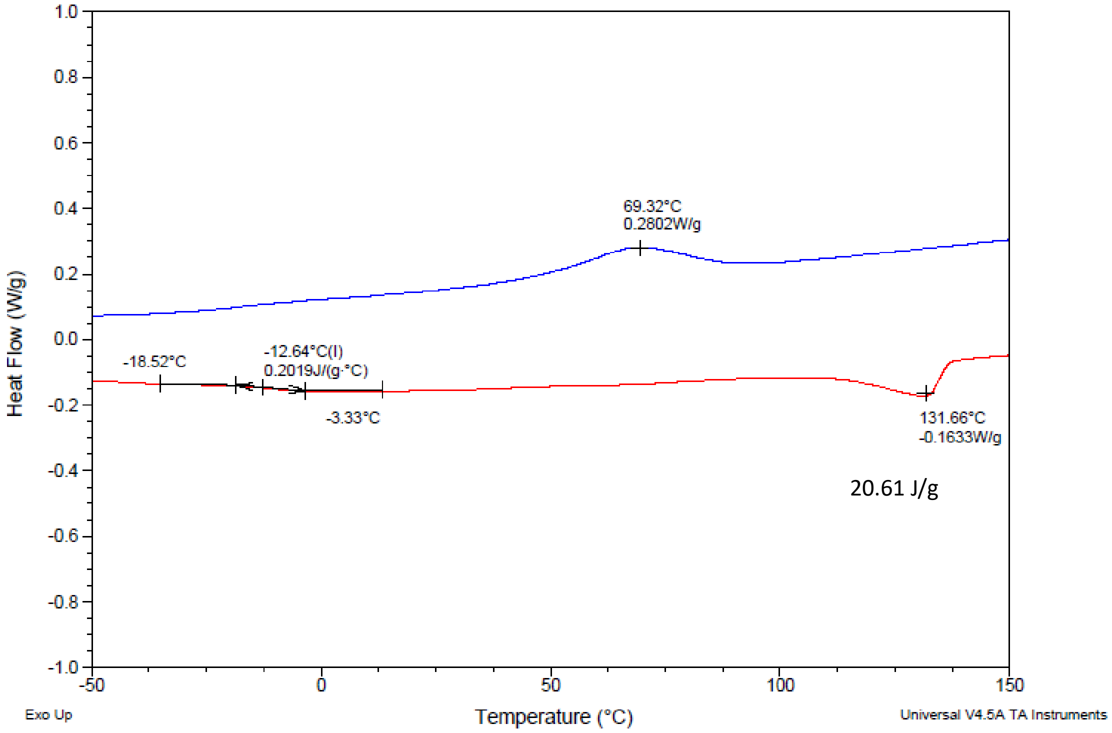

Figure S38. DSC Trace of 1,4-PBAF0.7. Experimental details in main manuscript. Displaying second heating cycle only, T_g and T_m determined from second heating cycle.

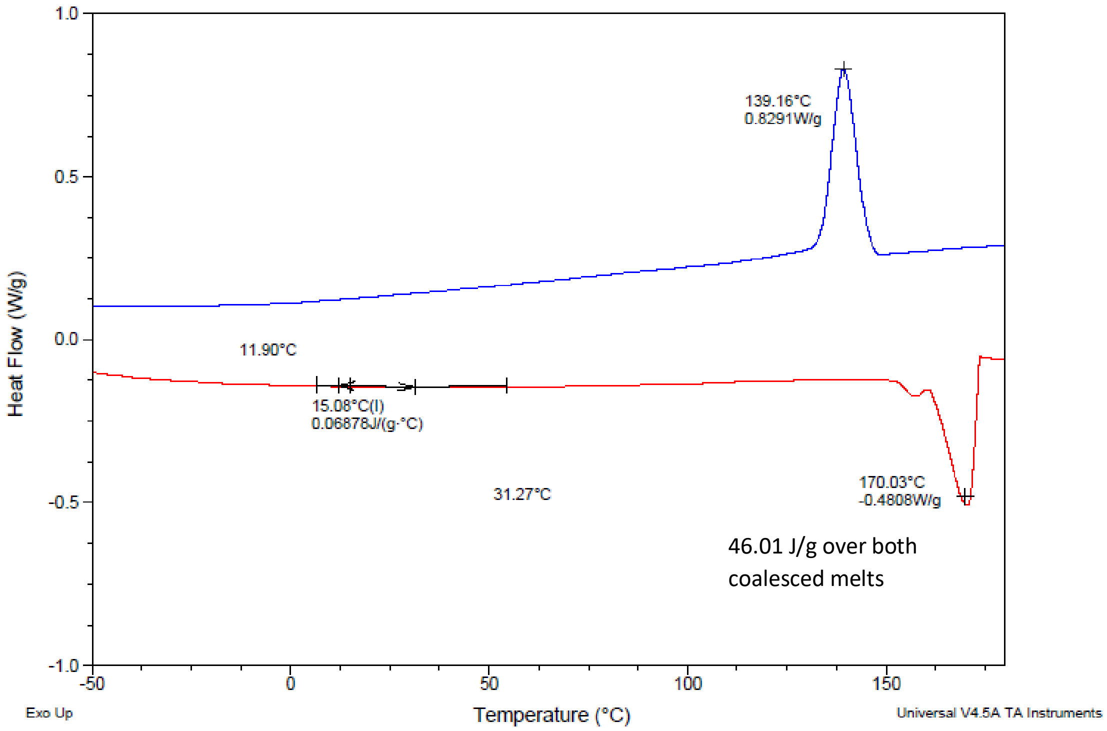

Figure S39. DSC Trace of 1,4-PBF. Experimental details in main manuscript. Displaying second heating cycle only, T_g and T_m determined from second heating cycle.

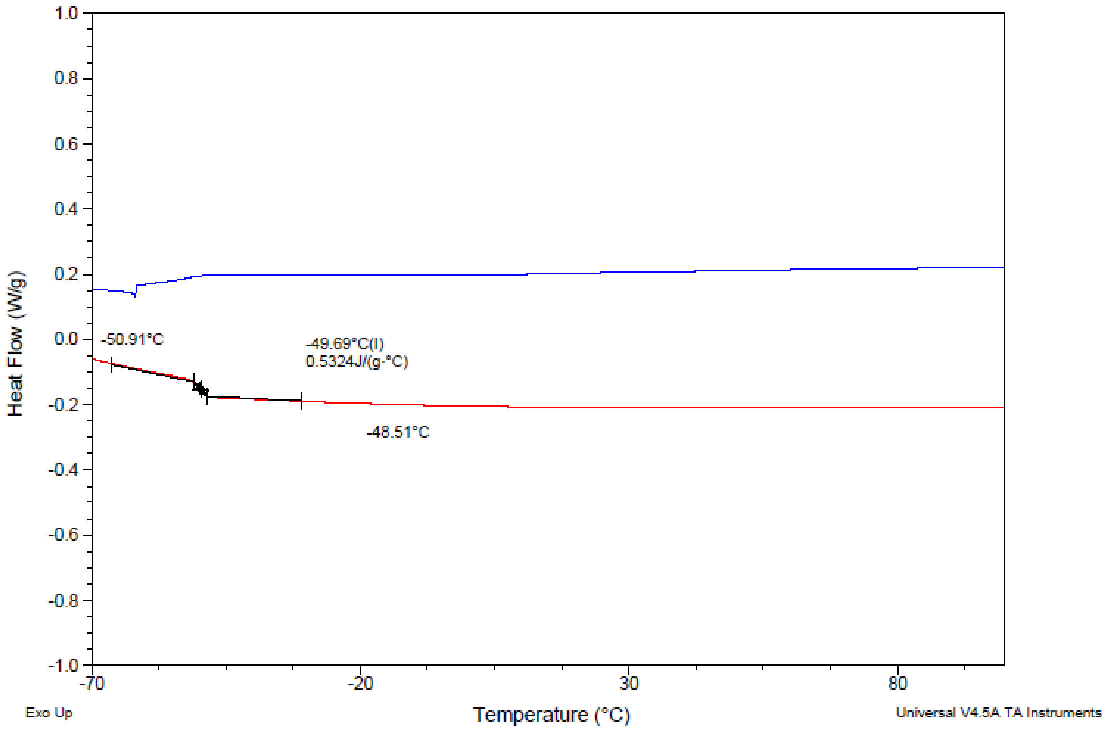

Figure S40. DSC Trace of 1,4-PPA. Experimental details in main manuscript. Displaying second heating cycle only, T_g and T_m determined from second heating cycle.

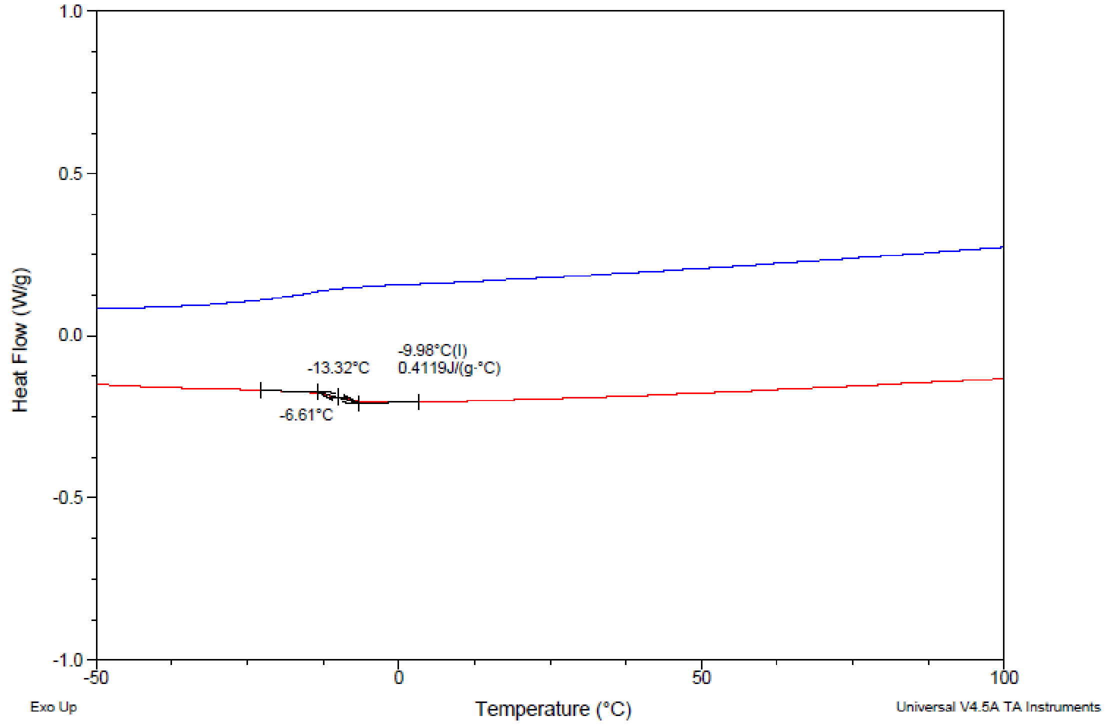

Figure S41. DSC Trace of 1,4-PPAF0.5. Experimental details in main manuscript. Displaying second heating cycle only, T_g and T_m determined from second heating cycle.

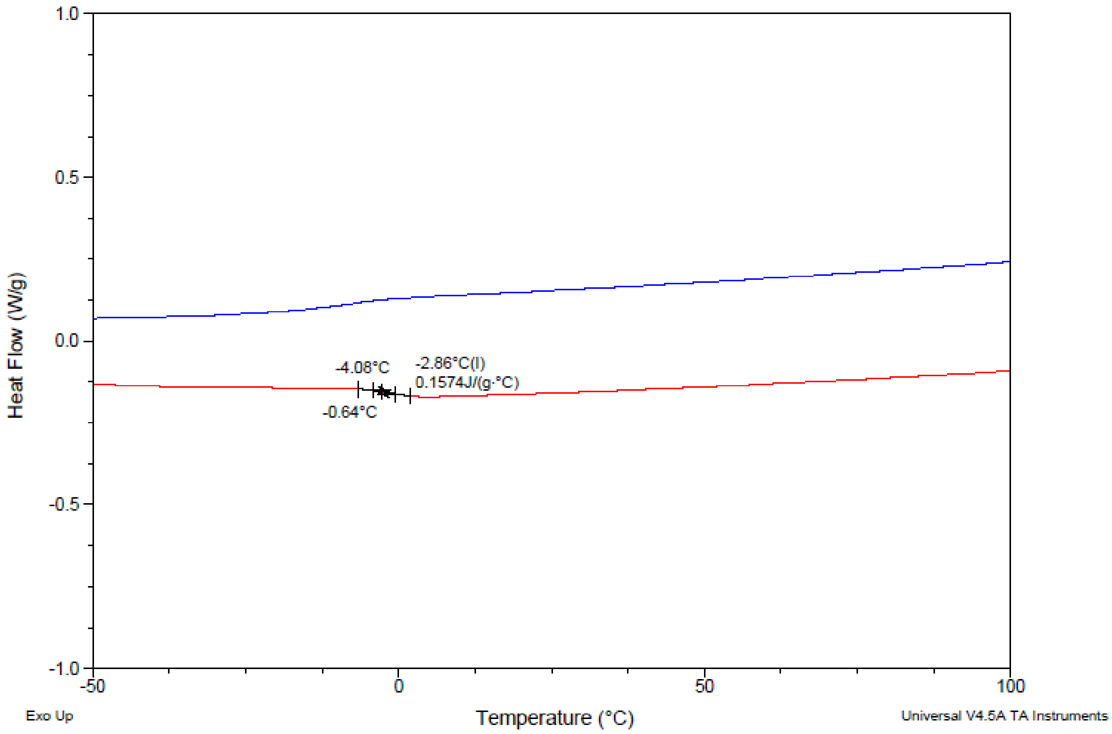

Figure S42. DSC Trace of 1,4-PPAF0.6. Experimental details in main manuscript. Displaying second heating cycle only, T_g and T_m determined from second heating cycle.

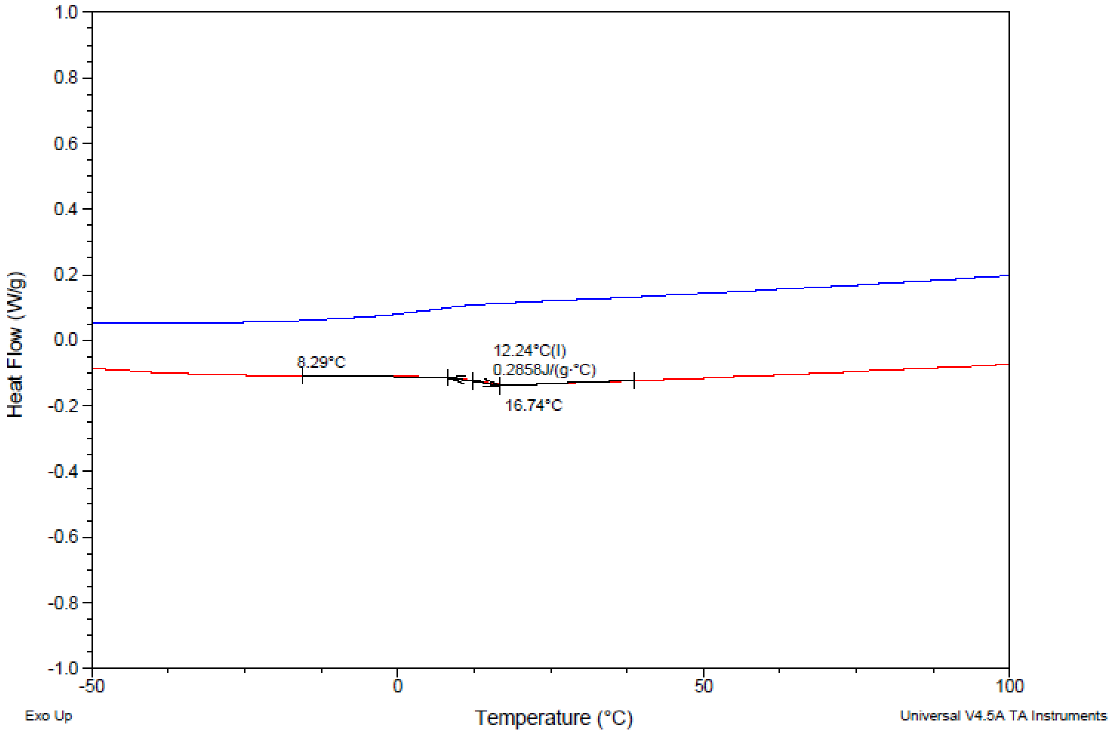

Figure S43. DSC Trace of 1,4-PPAF0.7. Experimental details in main manuscript. Displaying second heating cycle only, T_g and T_m determined from second heating cycle.

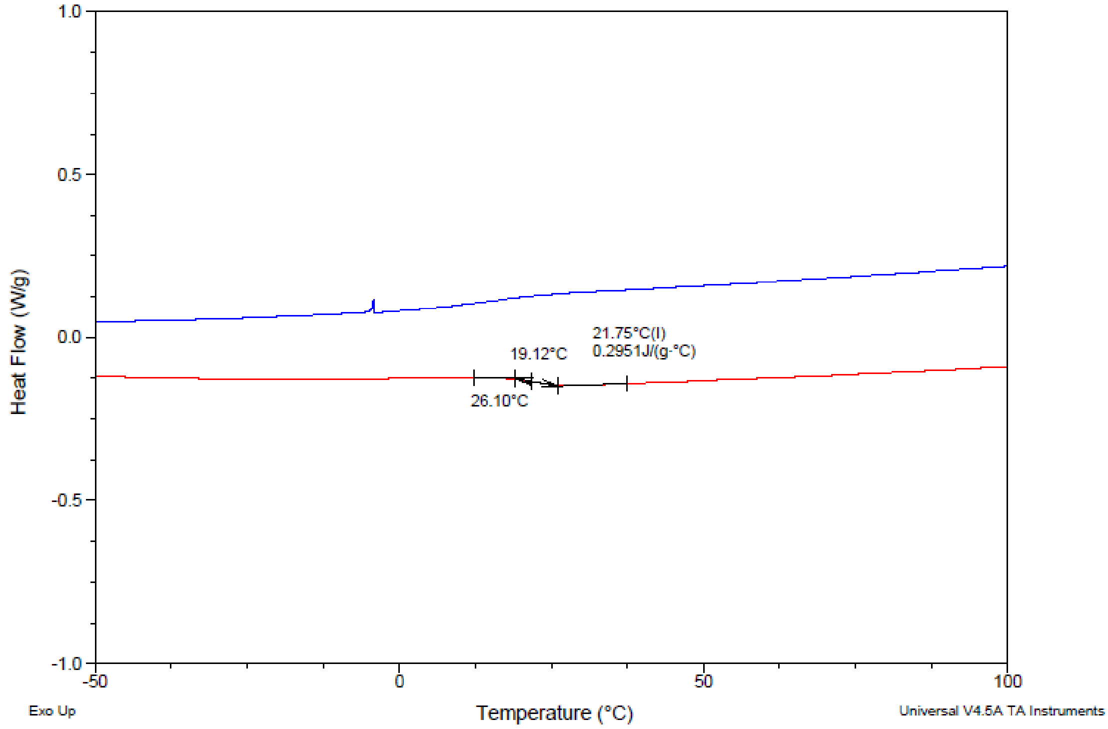

Figure S44. DSC Trace of 1,4-PPF. Experimental details in main manuscript. Displaying second heating cycle only, T_g and T_m determined from second heating cycle.

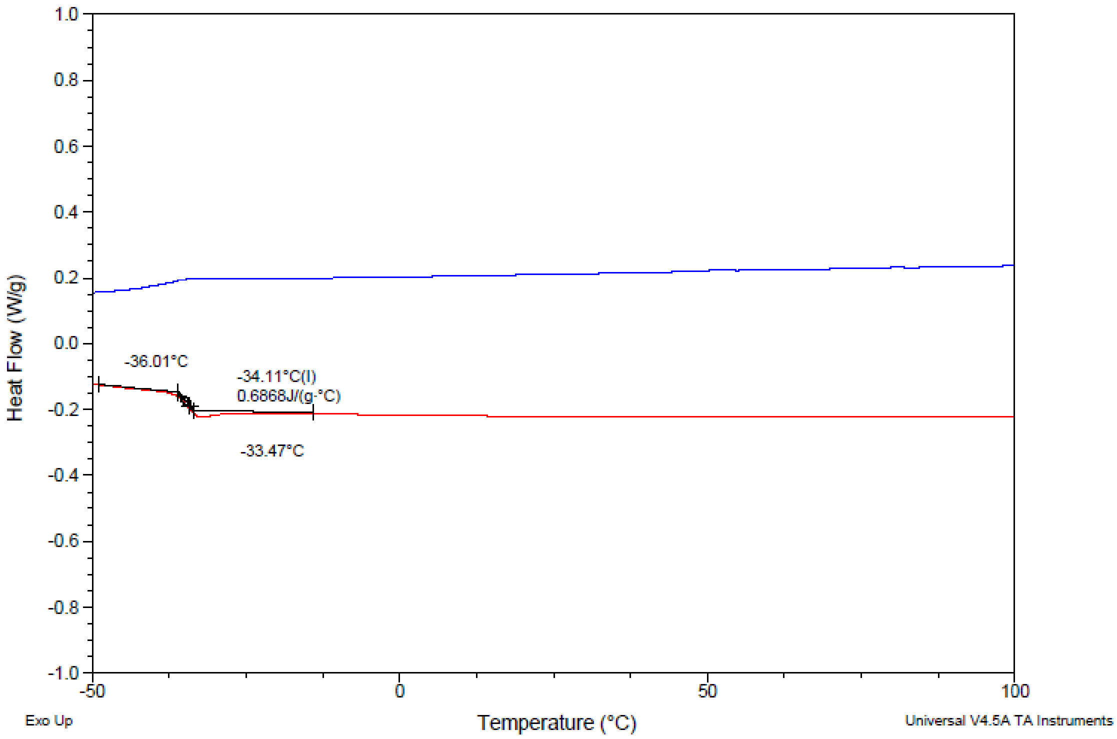

Figure S45. DSC Trace of 2,5-PHA. Experimental details in main manuscript. Displaying second heating cycle only, T_g and T_m determined from second heating cycle.

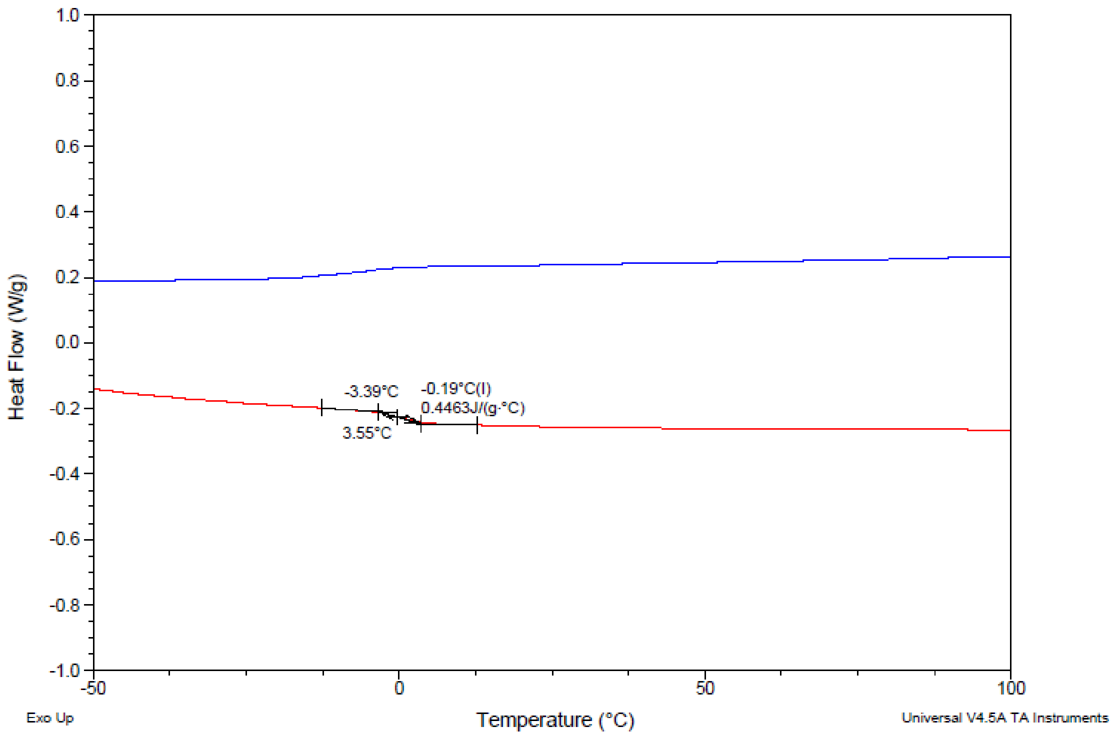

Figure S46. DSC Trace of 2,5-PHAF0.5. Experimental details in main manuscript. Displaying second heating cycle only, T_g and T_m determined from second heating cycle.

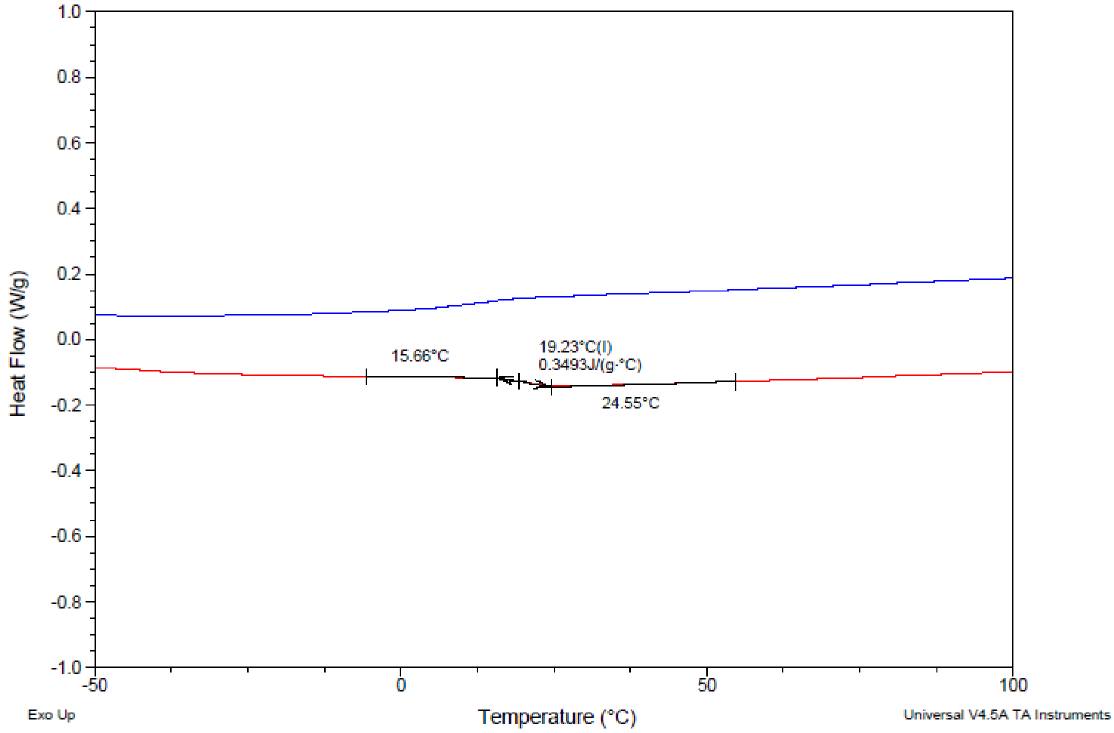

Figure S47. DSC Trace of 2,5-PHAF0.6. Experimental details in main manuscript. Displaying second heating cycle only, T_g and T_m determined from second heating cycle.

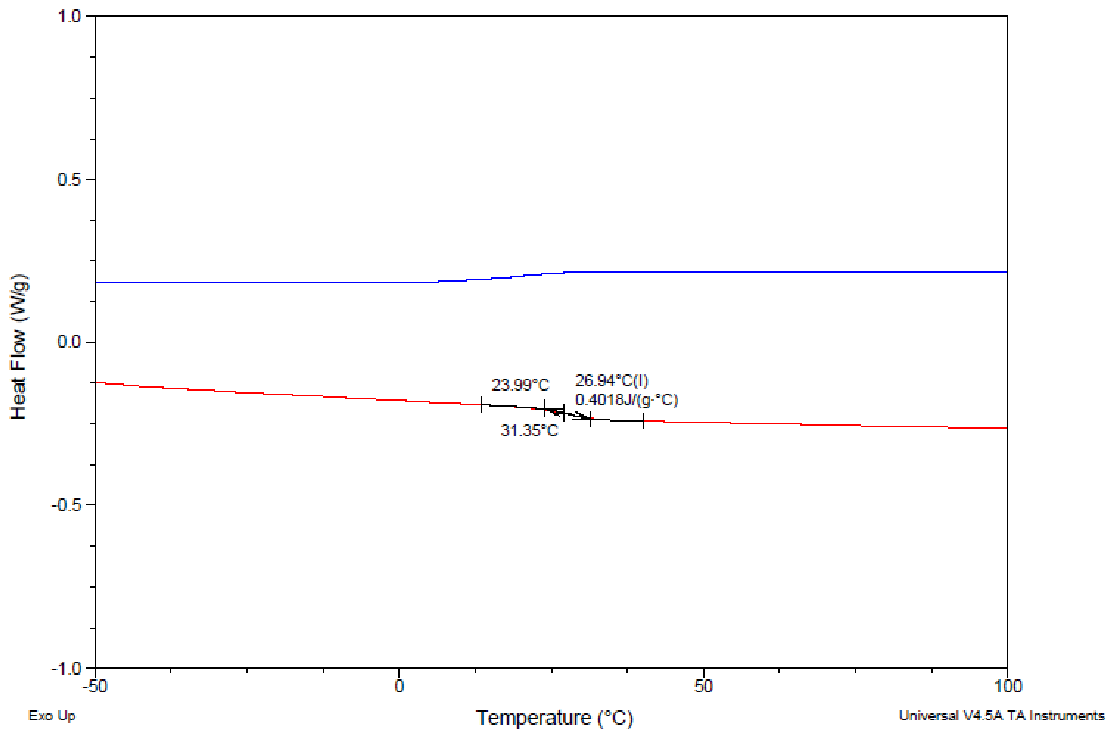

Figure S48. DSC Trace of 2,5-PHAF0.7. Experimental details in main manuscript. Displaying second heating cycle only, T_g and T_m determined from second heating cycle.

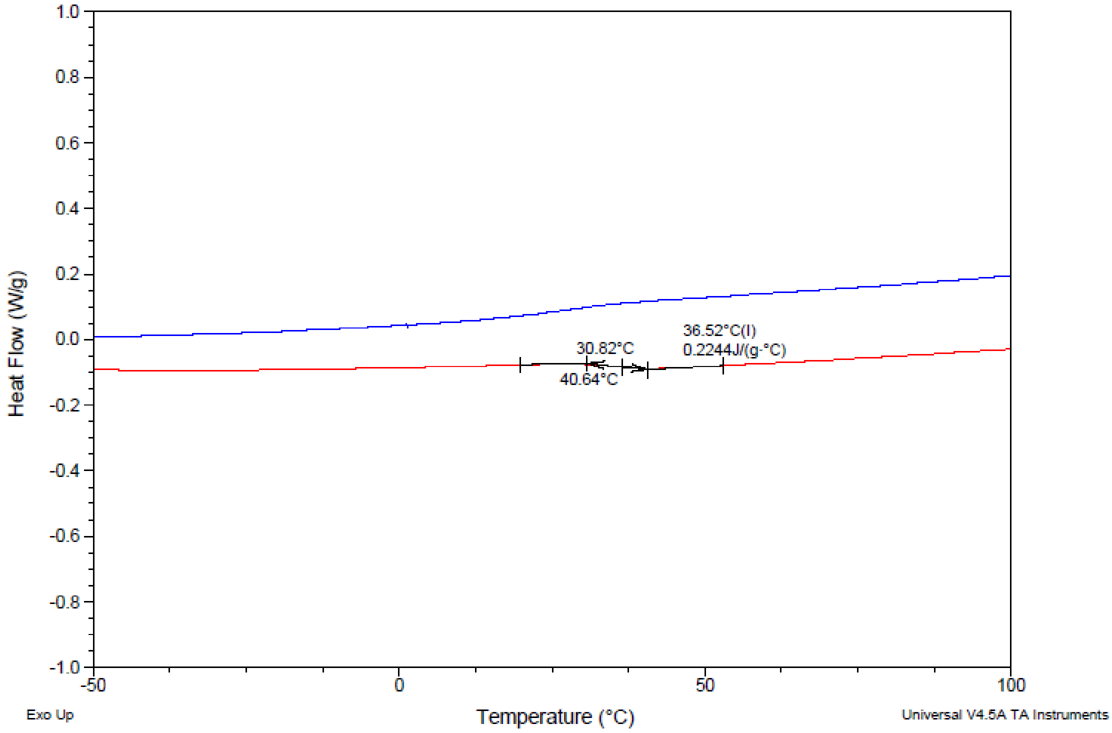

Figure S49. DSC Trace of 2,5-PHF. Experimental details in main manuscript. Displaying second heating cycle only, T_g and T_m determined from second heating cycle.

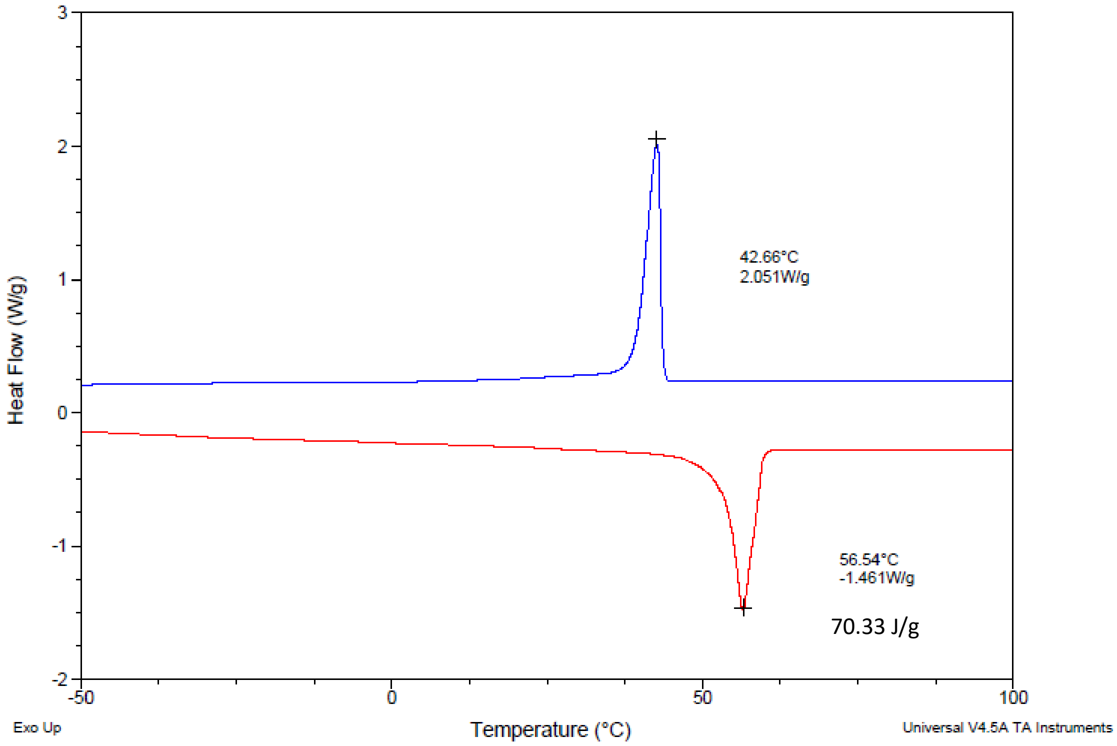

Figure S50. DSC Trace of 1,6-PHA. Experimental details in main manuscript. Displaying second heating cycle only, T_g and T_m determined from second heating cycle.

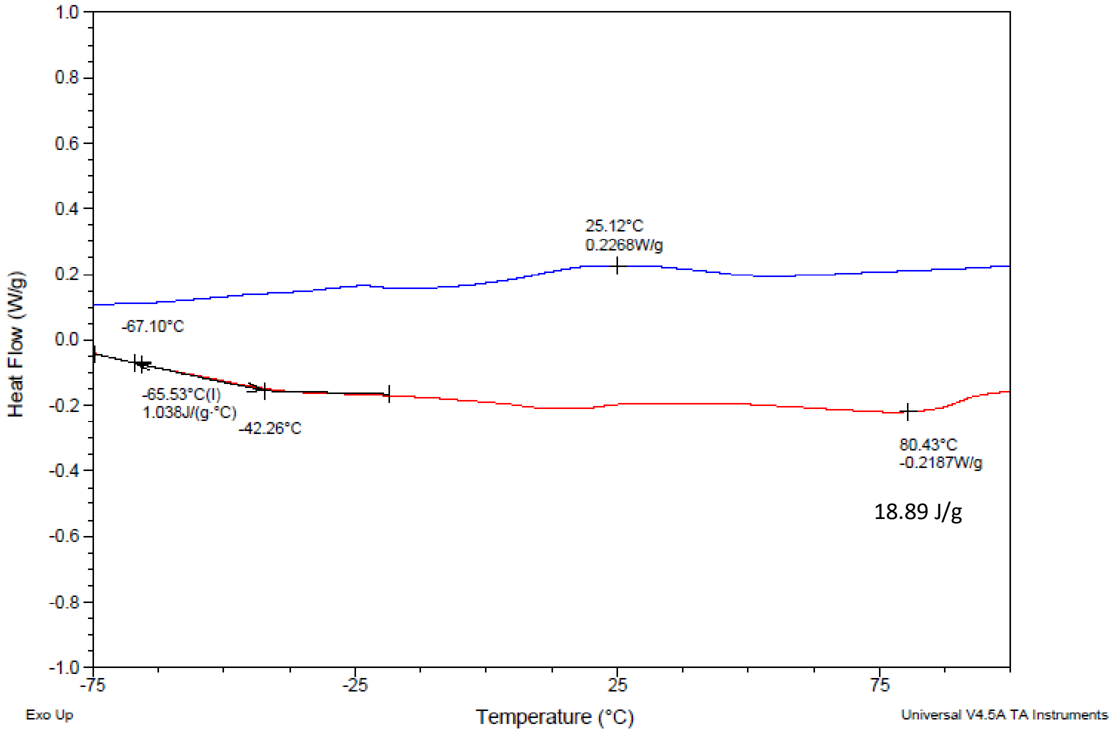

Figure S51. DSC Trace of 1,6-PHAF0.5. Experimental details in main manuscript. Displaying second heating cycle only, T_g and T_m determined from second heating cycle.

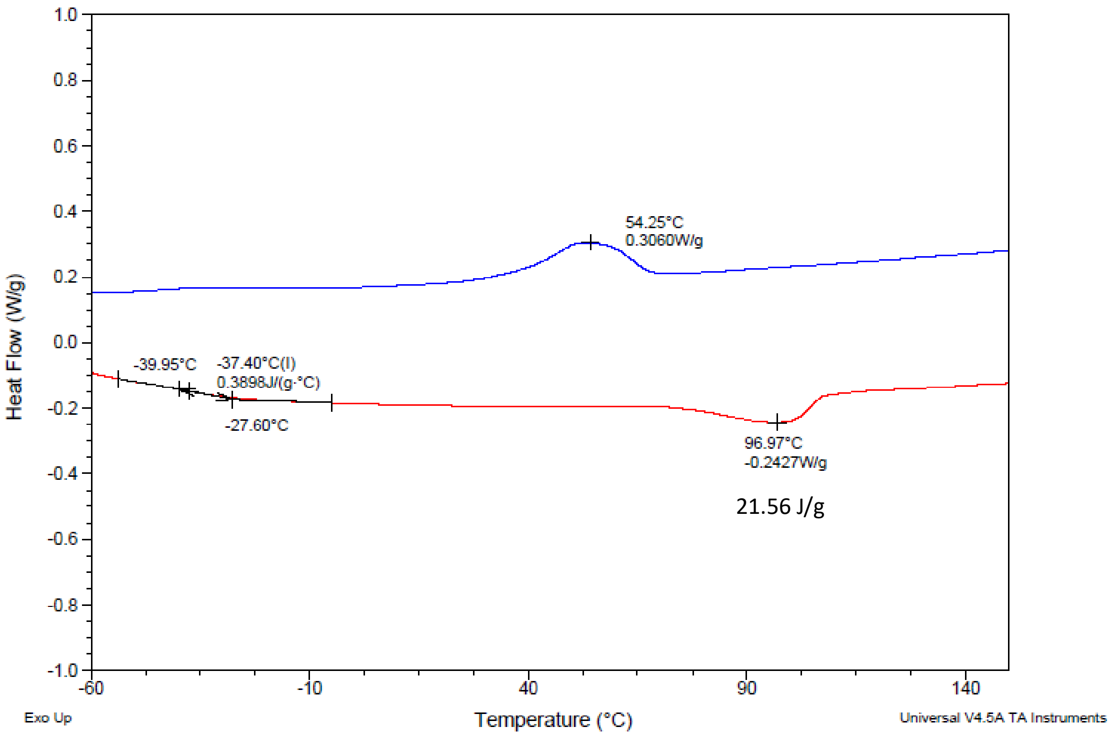

Figure S52. DSC Trace of 1,6-PHAF0.6. Experimental details in main manuscript. Displaying second heating cycle only, T_g and T_m determined from second heating cycle.

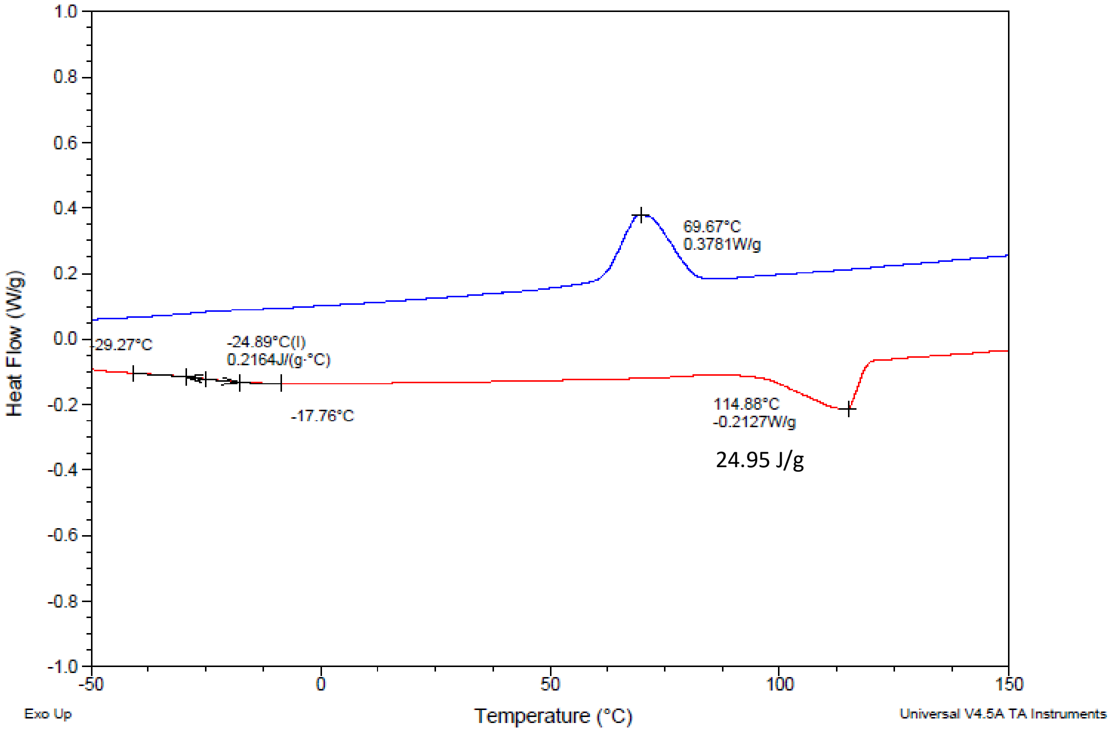

Figure S53. DSC Trace of 1,6-PHAF0.7. Experimental details in main manuscript. Displaying second heating cycle only, T_g and T_m determined from second heating cycle.

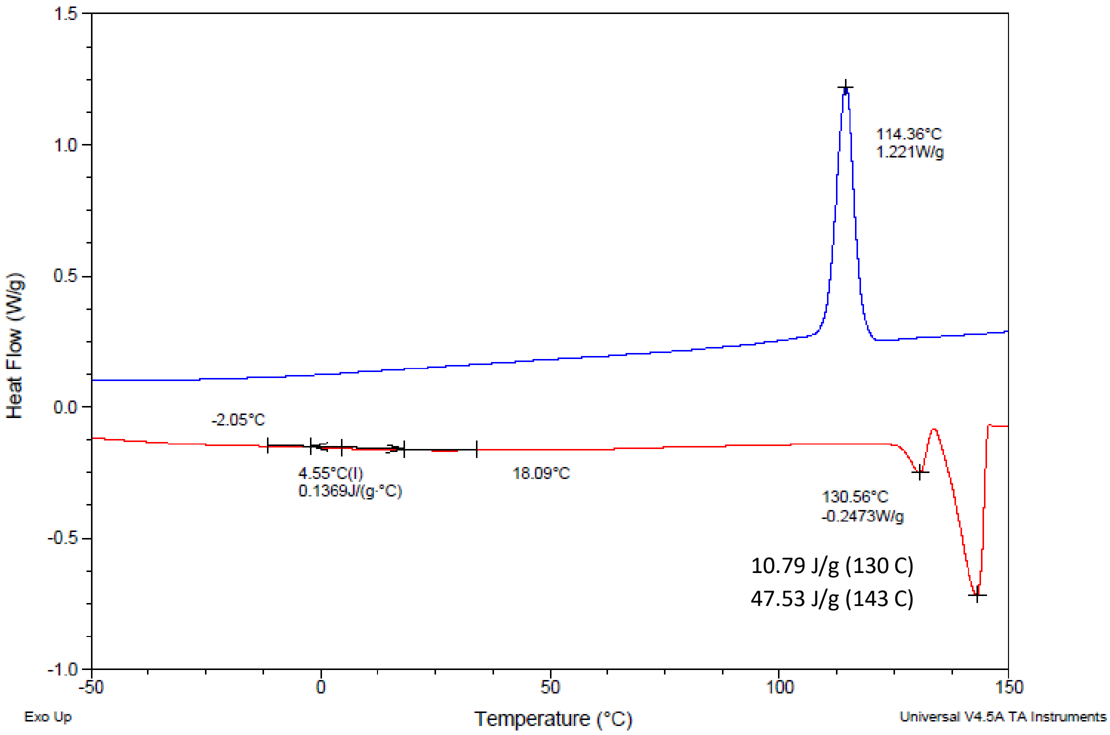

Figure S54. DSC Trace of 1,6-PHF. Experimental details in main manuscript. Displaying second heating cycle only, T_g and T_m determined from second heating cycle.

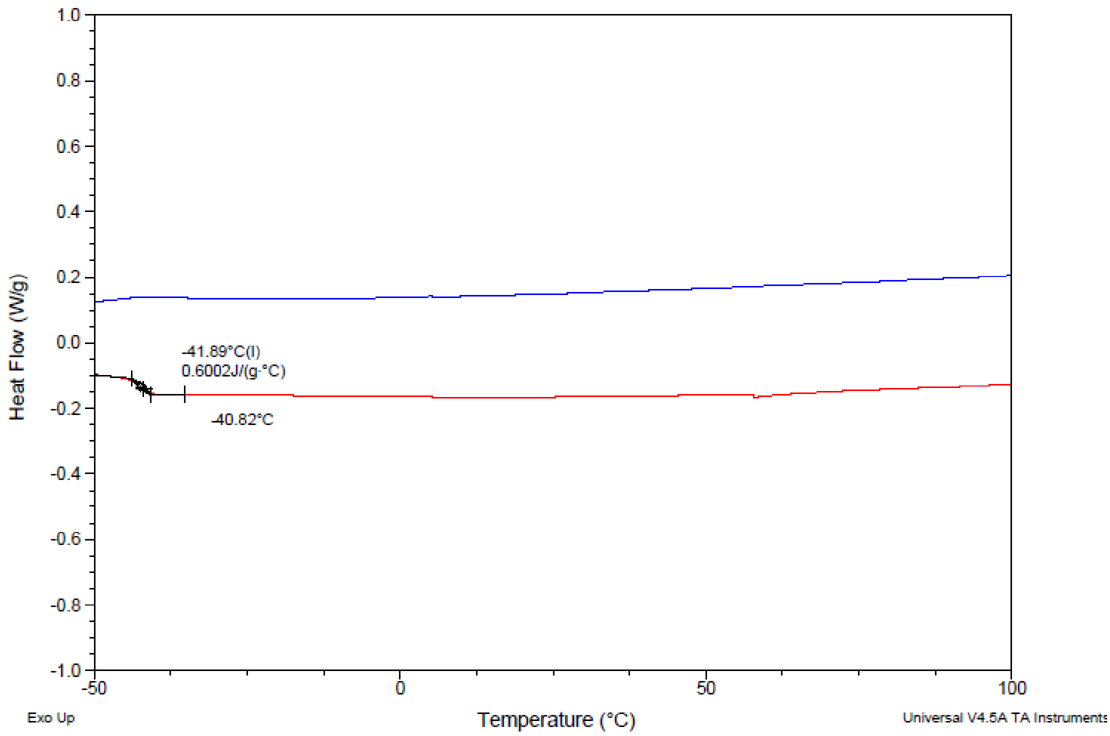

Figure S55. DSC Trace of 2,7-POA. Experimental details in main manuscript. Displaying second heating cycle only, T_g and T_m determined from second heating cycle.

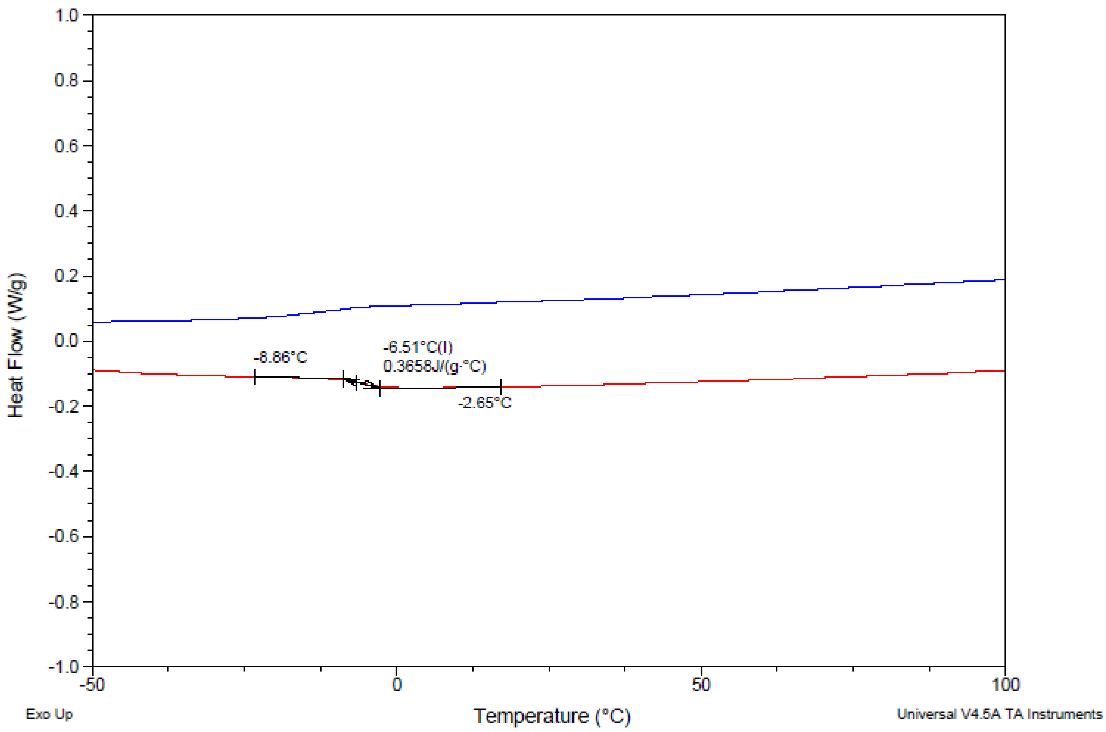

Figure S56. DSC Trace of 2,7-POAF0.5. Experimental details in main manuscript. Displaying second heating cycle only, T_g and T_m determined from second heating cycle.

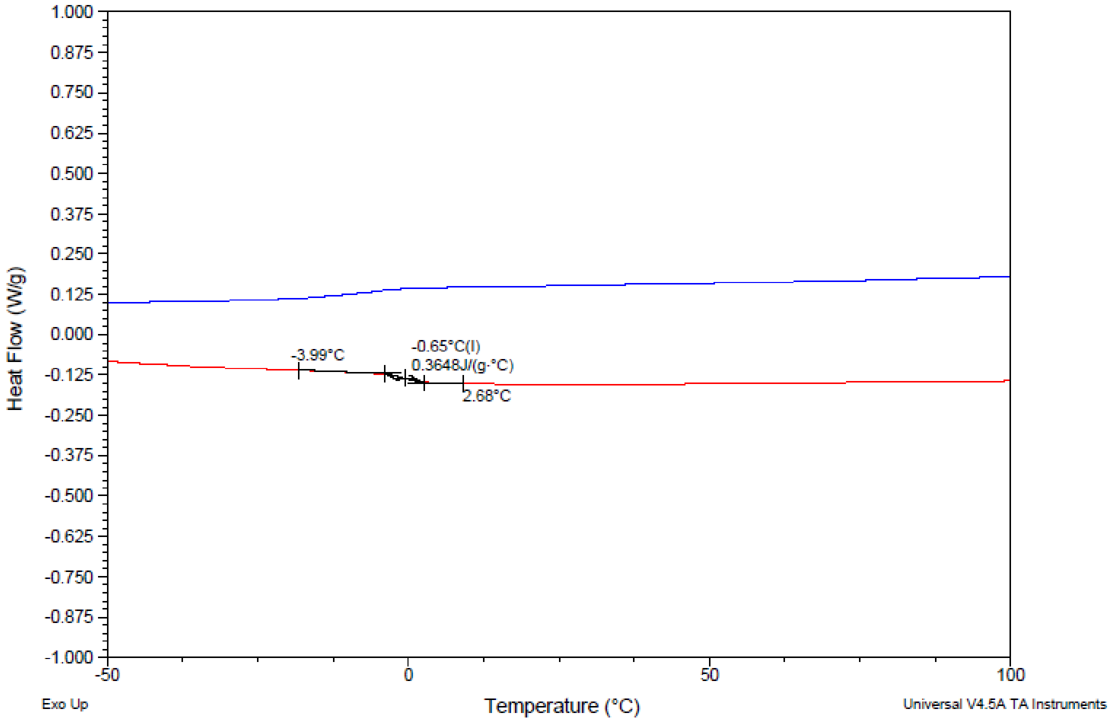

Figure S57. DSC Trace of 2,7-POAF0.6. Experimental details in main manuscript. Displaying second heating cycle only, T_g and T_m determined from second heating cycle.

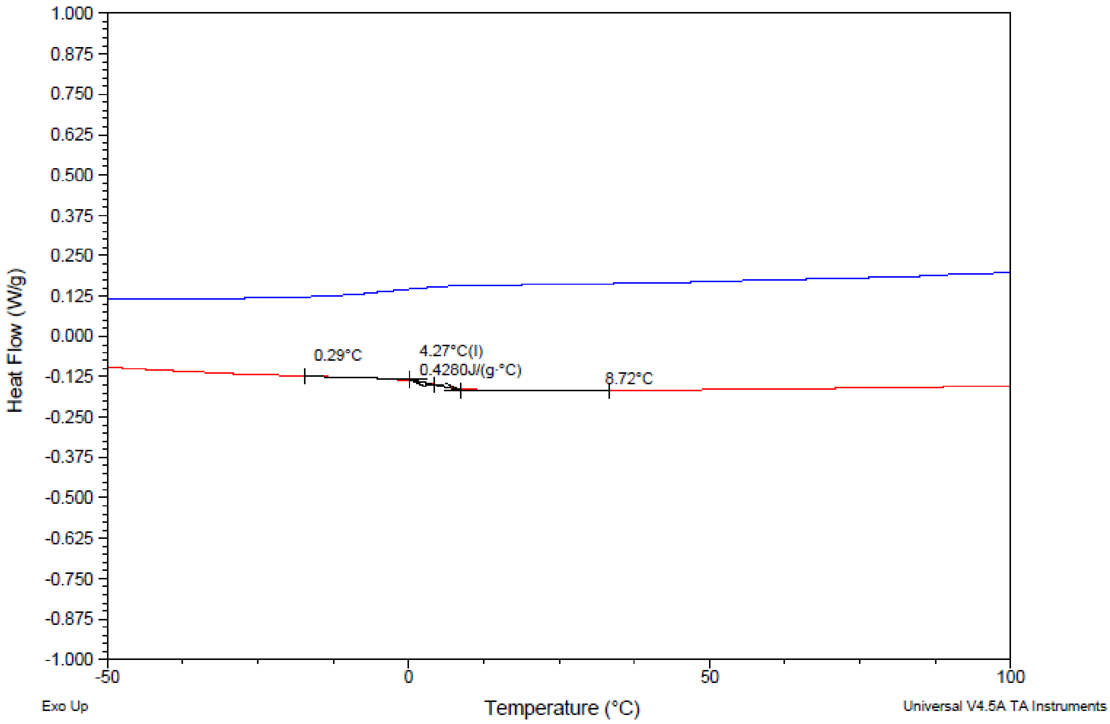

Figure S58. DSC Trace of 2,7-POAF0.7. Experimental details in main manuscript. Displaying second heating cycle only, T_g and T_m determined from second heating cycle.

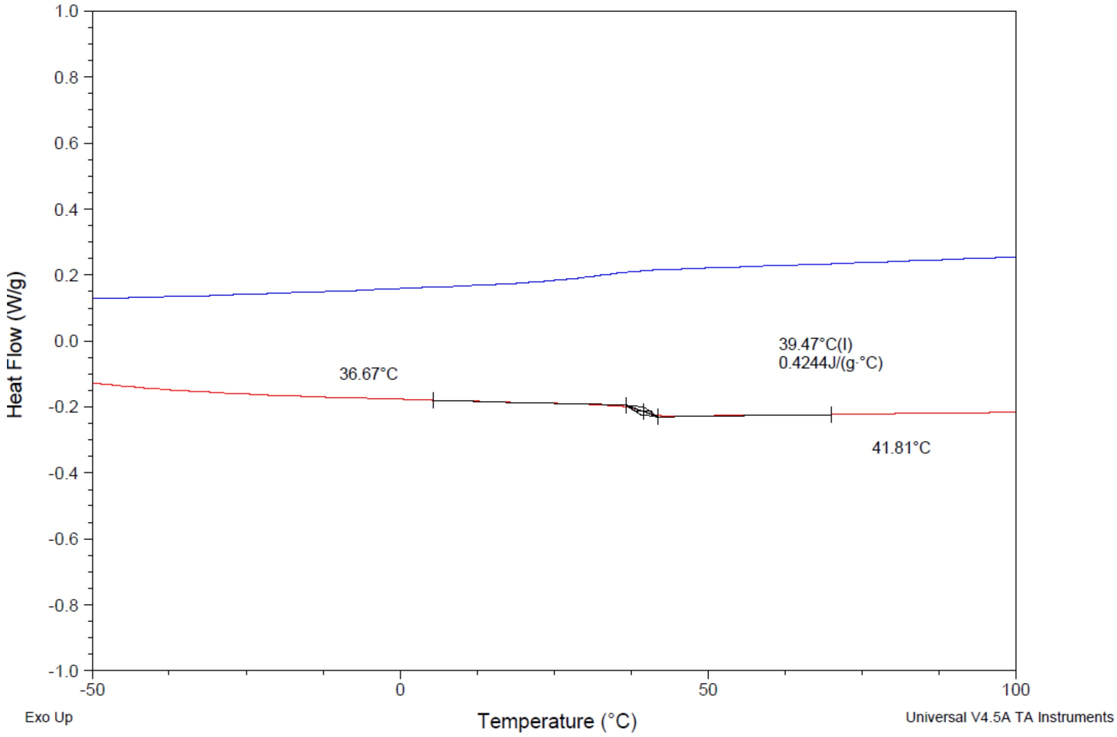

Figure S59. DSC Trace of 2,7-POF. Experimental details in main manuscript. Displaying second heating cycle only, T_g and T_m determined from second heating cycle.

S7. Visual Appearance of Polyesters from Optimised Reaction Conditions

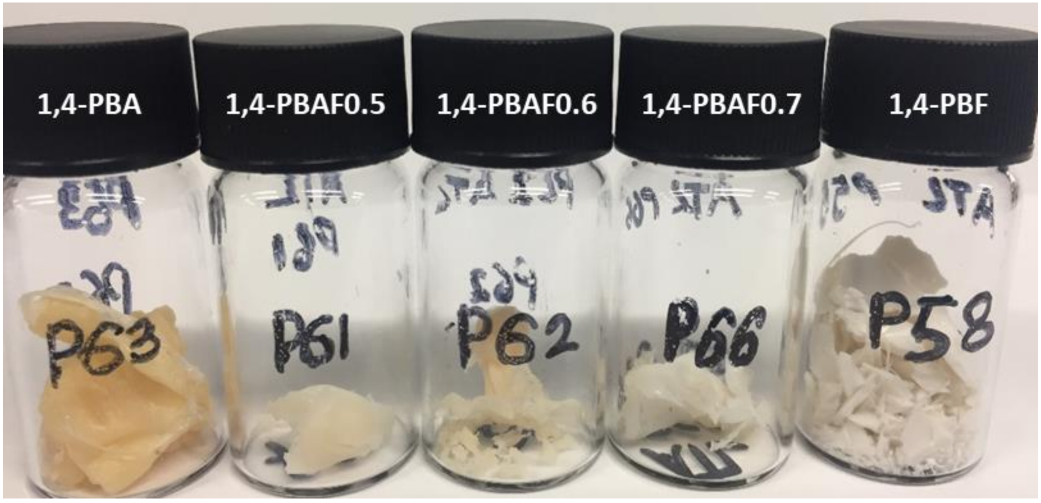

Figure S60. 1,4-PBAF series.

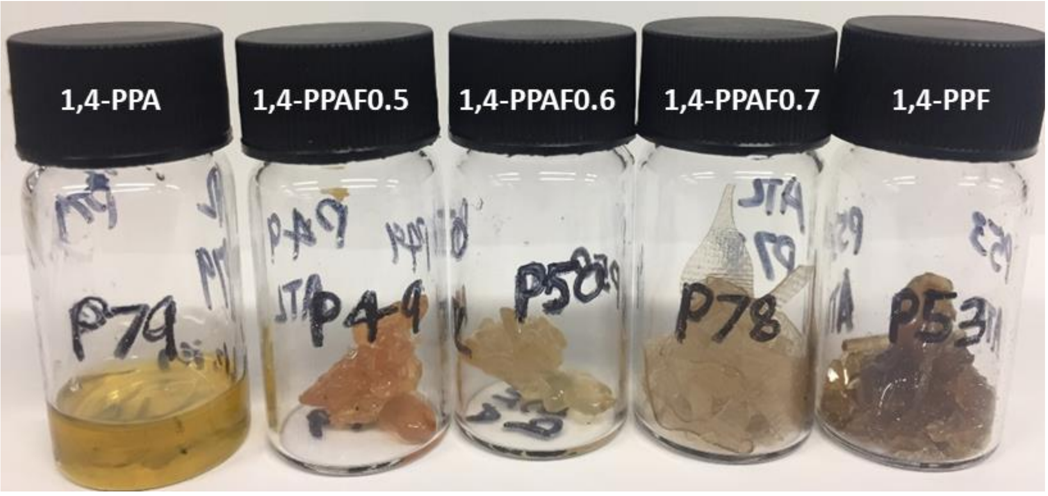

Figure S61. 1,4-PPAF series.

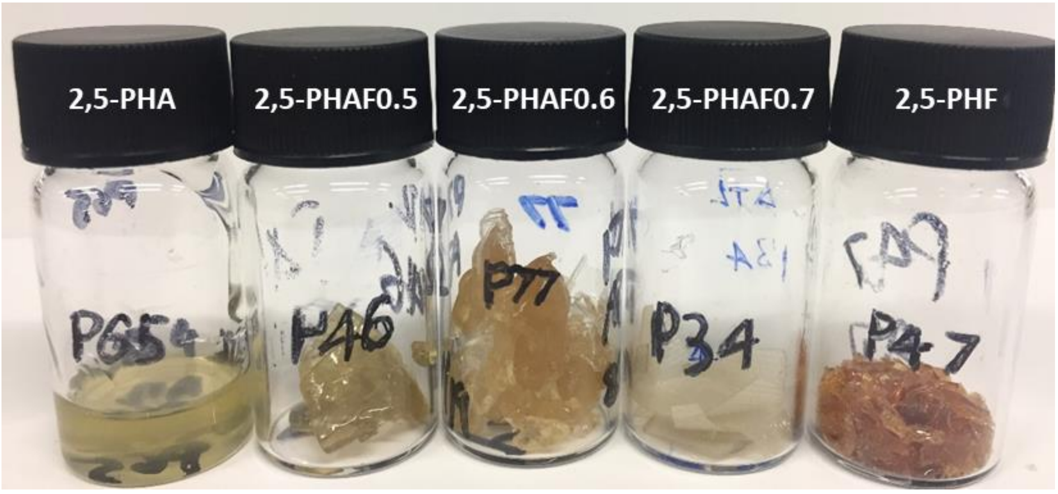

Figure S62. 2,5-PHAF series.

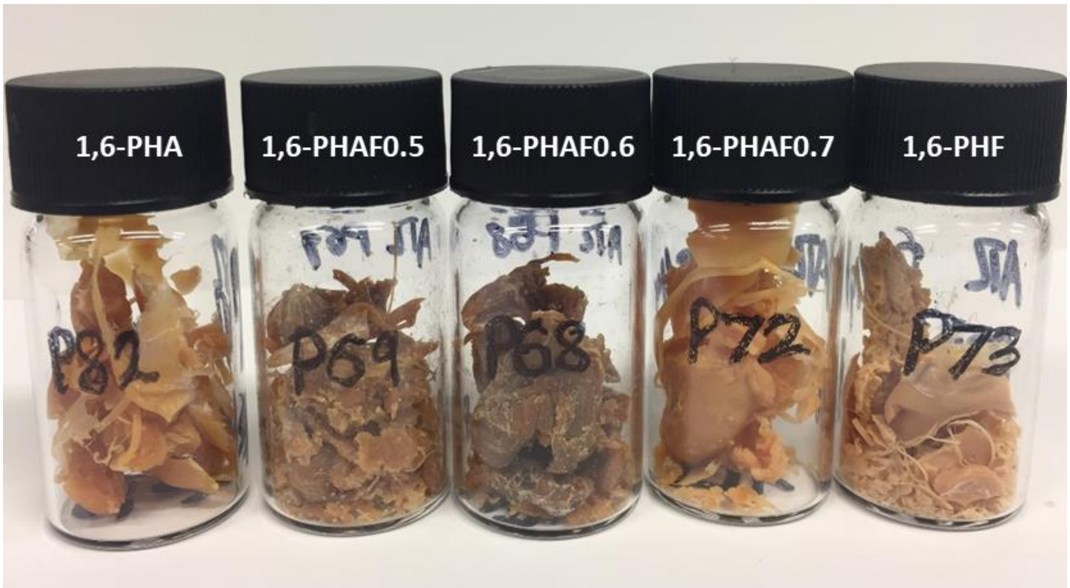

Figure S63. 1,6-PHAF series.

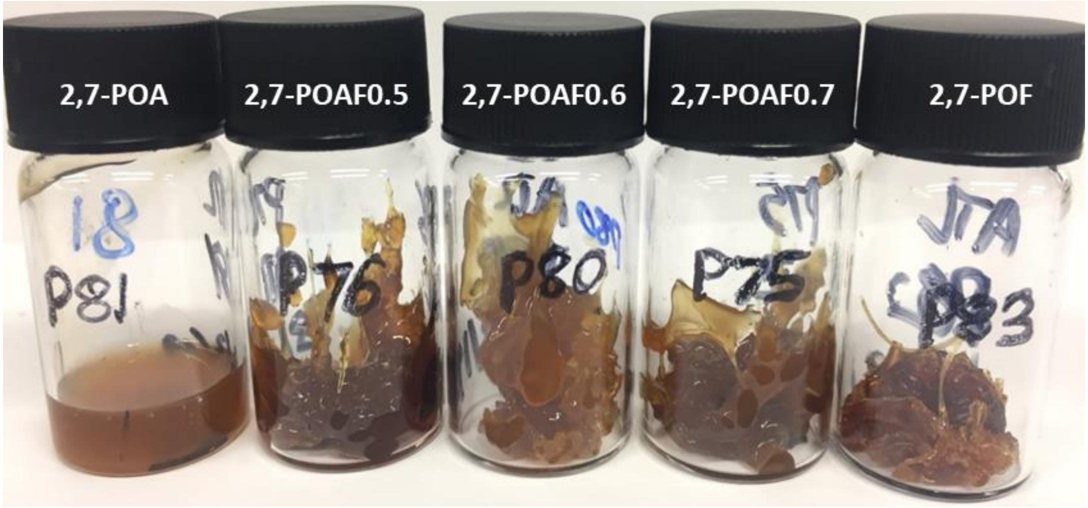

Figure S64. 2,7-POAF series.

S8. Thickness of Films Prepared

Table S9. Film thickness range following multiple measurements over the film sample

Polymer	**Film thickness / mm**
1,4-PBAF0.6	0.27 - 0.29
1,4-PBAF0.7	0.32 - 0.34
1,4-PPAF0.7	0.28 - 0.32
2,5-PHAF0.6	0.26 - 0.30
2,5-PHAF0.7	0.32 - 0.34
1,6-PHAF0.7	0.28 – 0.30
2,7-POAF0.7	0.28 – 0.30

S9. Tensile Property Study of Polyester Films

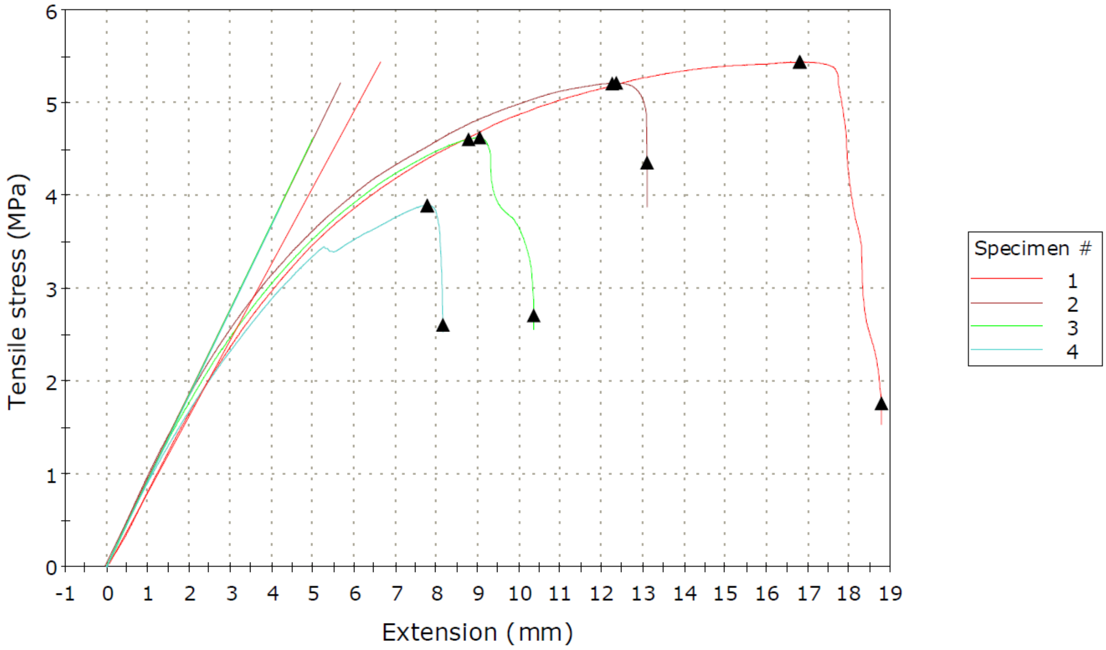

Figure S65. 1,4-PBAF0.6 Tensile Stress vs. Extension. Recorded on an Instron 3367 fitted with a 100 N (max) static load cell and screw action rubber grip claws. Four specimen dumbbells studied of dimension 0.3 x 20 x 3 mm (with 10 x 10 mm squares as gripping sites at either end). 5 mm/min extension at ambient temperature and pressure.

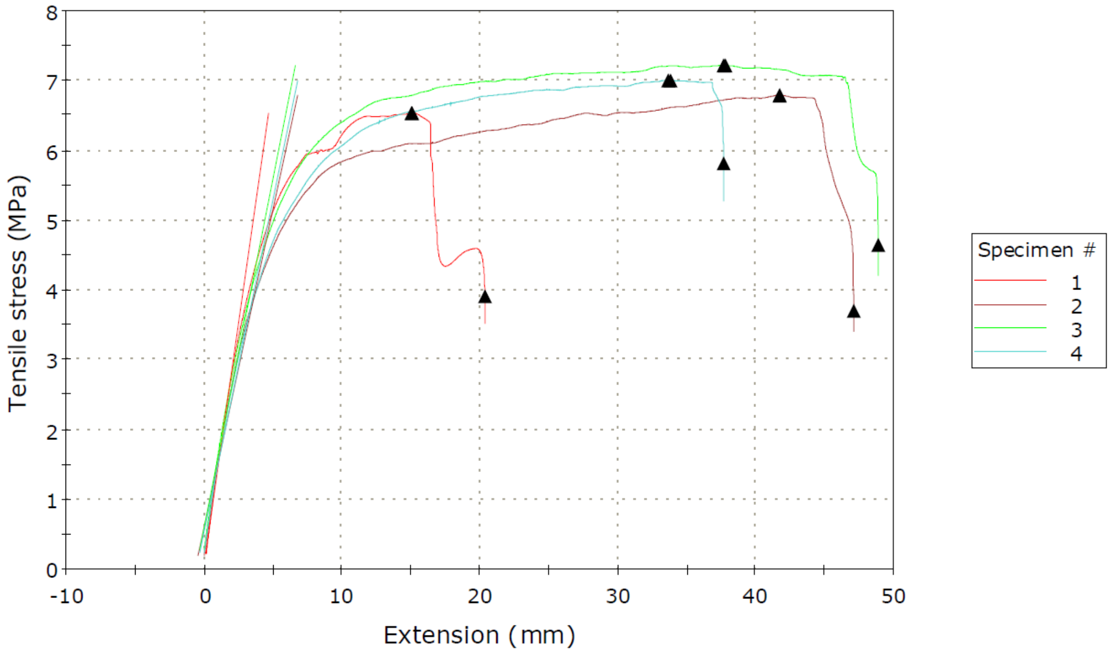

Figure S66. 1,4-PBAF0.7 Tensile Stress vs. Extension. Recorded on an Instron 3367 fitted with a 100 N (max) static load cell and screw action rubber grip claws. Four specimen dumbbells studied of dimension 0.3 x 20 x 3 mm (with 10 x 10 mm squares as gripping sites at either end). 5 mm/min extension at ambient temperature and pressure.

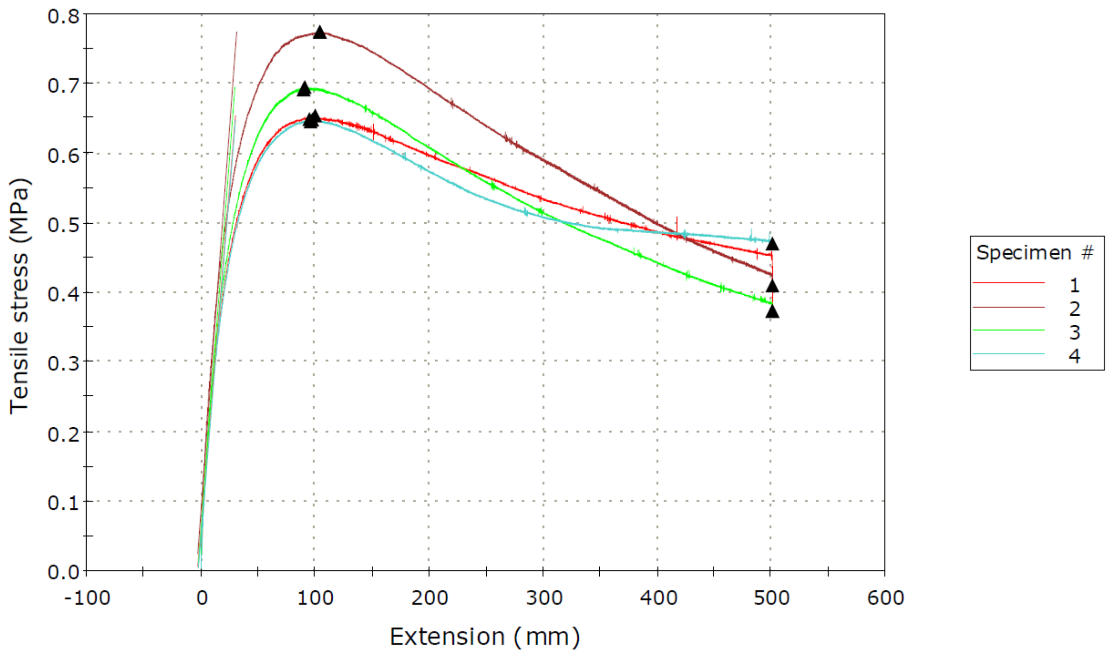

Figure S67. 1,4-PPAF0.7 Tensile Stress vs. Extension. Recorded on an Instron 3367 fitted with a 100 N (max) static load cell and screw action rubber grip claws. Four specimen dumbbells studied of dimension 0.3 x 20 x 3 mm (with 10 x 10 mm squares as gripping sites at either end). 5 mm/min extension at ambient temperature and pressure. **Instrument run to maximum extension of 500 mm.**

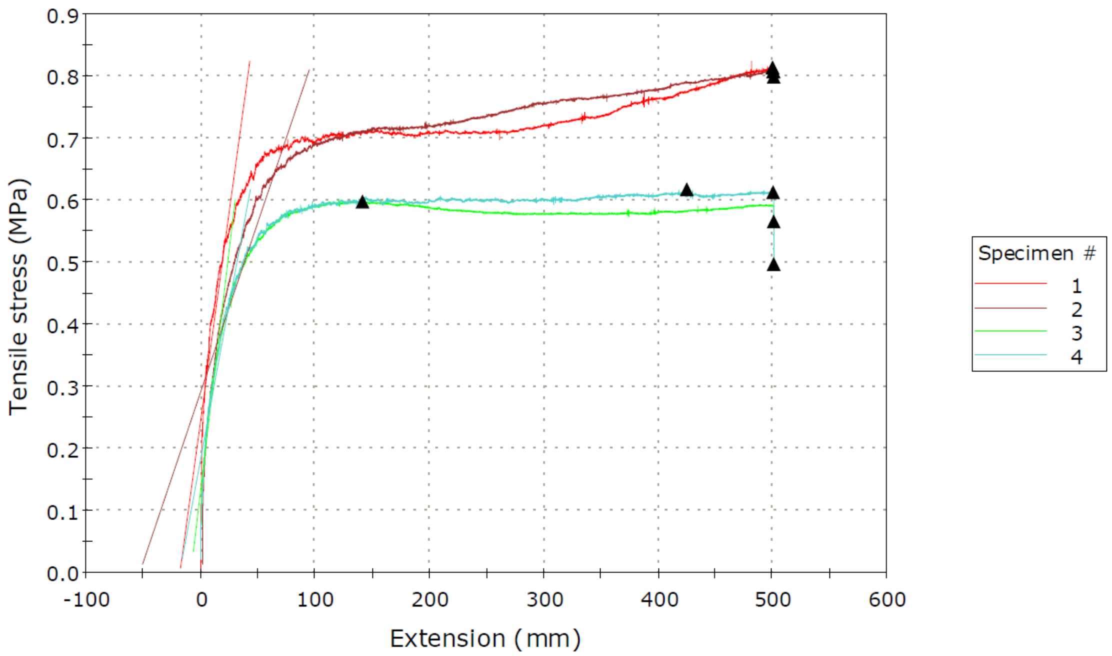

Figure S68. 2,5-PHAF0.6 Tensile Stress vs. Extension. Recorded on an Instron 3367 fitted with a 100 N (max) static load cell and screw action rubber grip claws. Four specimen dumbbells studied of dimension 0.3 x 20 x 3 mm (with 10 x 10 mm squares as gripping sites at either end). 5 mm/min extension at ambient temperature and pressure **Instrument run to maximum extension of 500 mm.**

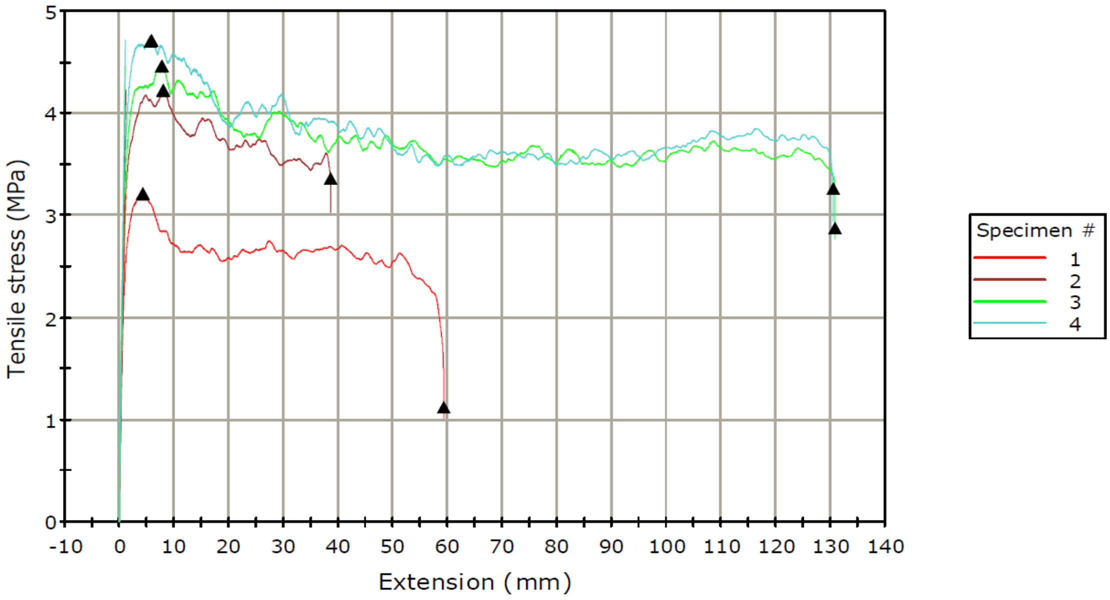

Figure S69. 2,5-PHAF0.7 (entry 5, Table 2 in main manuscript) Tensile Stress vs. Extension. Recorded on an Instron 3367 fitted with a 100 N (max) static load cell and screw action rubber grip claws. Four specimen dumbbells studied of dimension 0.3 x 20 x 3 mm (with 10 x 10 mm squares as gripping sites at either end). 5 mm/min extension at ambient temperature and pressure.

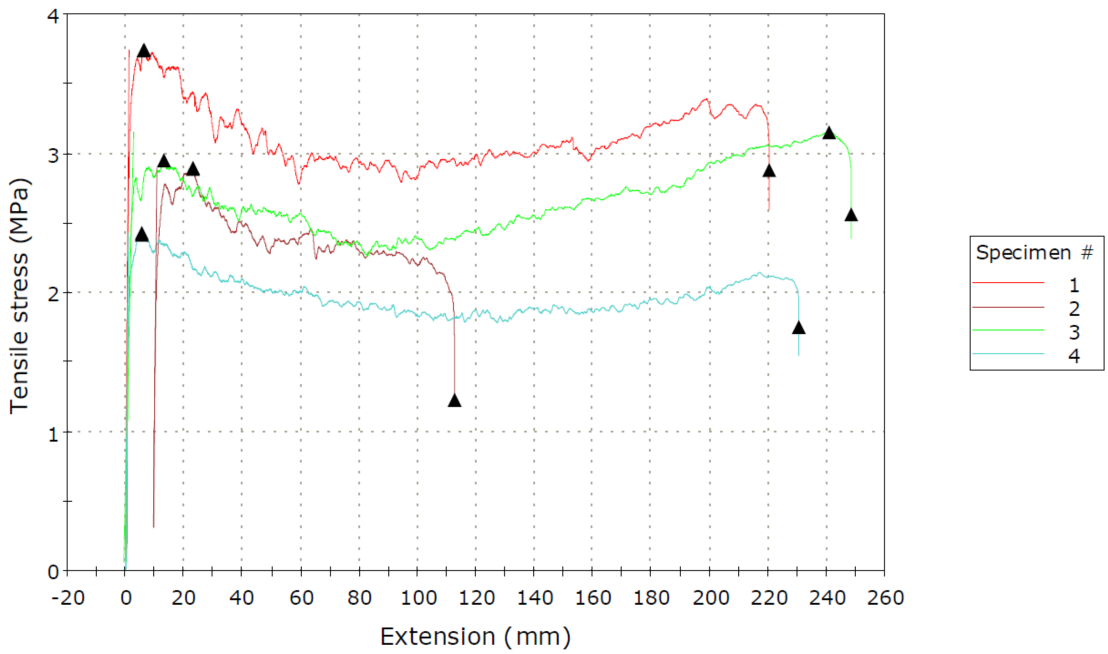

Figure S70. 2,5-PHAF0.7 (entry 6, Table 2 in main manuscript) Tensile Stress vs. Extension. Recorded on an Instron 3367 fitted with a 100 N (max) static load cell and screw action rubber grip claws. Four specimen dumbbells studied of dimension 0.3 x 20 x 3 mm (with 10 x 10 mm squares as gripping sites at either end). 5 mm/min extension at ambient temperature and pressure.

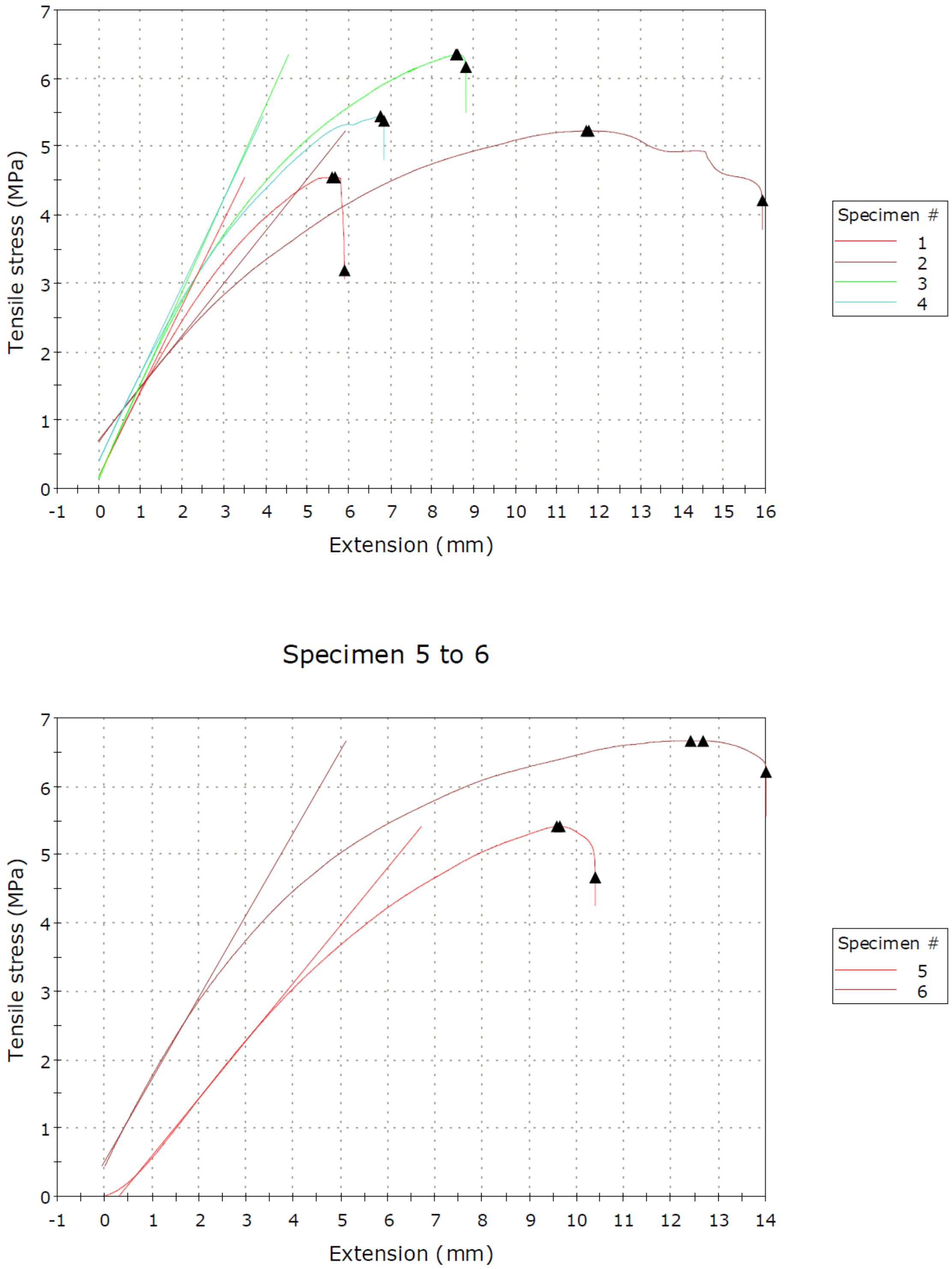

Figure S71. 1,6-PHAF0.7 Tensile Stress vs. Extension. Recorded on an Instron 3367 fitted with a 100 N (max) static load cell and screw action rubber grip claws. Six specimen dumbbells studied of dimension 0.3 x 20 x 3 mm (with 10 x 10 mm squares as gripping sites at either end). 5 mm/min extension at ambient temperature and pressure.

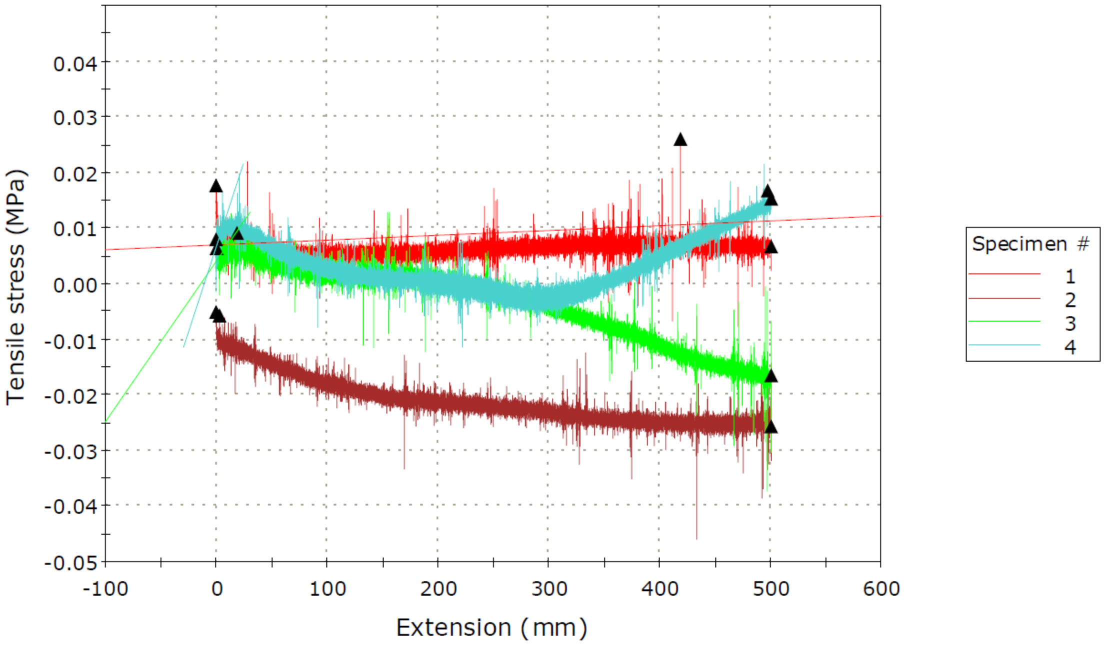

Figure S72. 2,7-POAF0.7 Tensile Stress vs. Extension. Recorded on an Instron 3367 fitted with a 100 N (max) static load cell and screw action rubber grip claws. Four specimen dumbbells studied of dimension 0.3 x 20 x 3 mm (with 10 x 10 mm squares as gripping sites at either end). 5 mm/min extension at ambient temperature and pressure.

S10. Trends in Water Contact Angle vs Furan Content and Polyester Chain Length

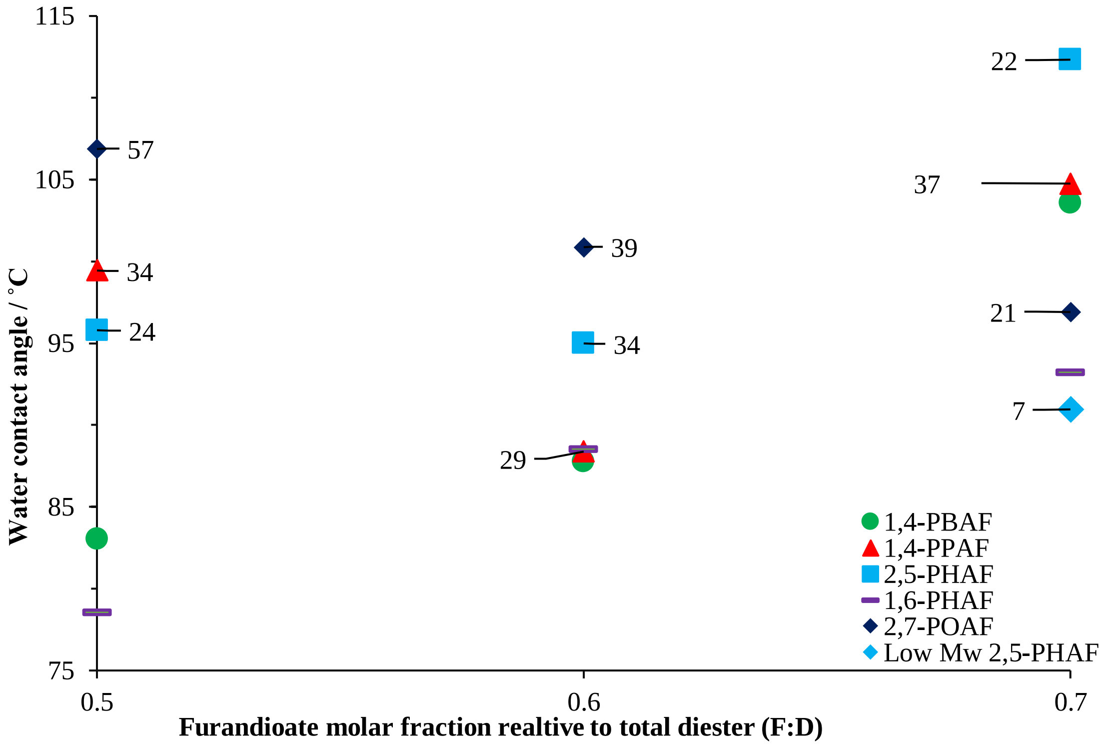

Figure S73. Graph displaying the water contact angles. Method for water contact angle determination is detailed in experimental section of main manuscript. Data labels represent M_w values in kDa determined by GPC, those without values were insoluble in the GPC solvent.

S11. Polyester Synthesis Using CaLB Enzyme as Catalyst

Table S10. Enzyme Catalysed Synthesis of Adipate Polyesters With 2º Alcohol Diols

Diol	NMR Conversion [%]		GPC		
	Diol	**Ester**	**M_n**	**M_w**	**Đ**
2,3-BDO	96	96	1.5 kDa	2.4 kDa	2.10
2,5-HDO	82	97	1.2 kDa	2.4 kDa	2.06
2,7-ODO	83	99	1.4 kDa	2.9 kDa	2.06

0.006 mol of dimethyl adipate (1.045 g) and 0.006 mol of diol (2,3-butanediol (2,3-BDO), 2,5-hexanediol (2,5-HDO) or 2,7-octanediol (2,7-ODO), diester:diol ratio = 1.0:1.0) were accurately weighted in a 25 mL round bottom flask. The mixture was then stirred at 85 °C until a homogeneous melt was obtained. 10% w w^{-1} (calculated on the total amount of the monomers) of immobilised CaLB N435 was then added and the reaction was run for 6 h at 1 atm. A vacuum of 20 mbar was subsequently applied for an additional 18 h maintaining the reaction temperature at 85 °C (total reaction time: 24 h). The reaction product was recovered by adding DCM in order to dissolve the solid reaction products. The biocatalyst was then removed *via* a filtration step and the solvent evaporated under vacuum. The polymers were then characterised without additional purification steps.

S12. References

1. Hunt, A. J.; Farmer, T. J.; Clark, J. H., Chapter 1: Elemental Sustainability and the Importance of Scarce Element Recovery. In *Element Recovery and Sustainability*, 1st Ed. ed.; Hunt, A. J., Ed. The Royal Society of Chemistry: Cambridge, 2013; pp 1-28.
2. Titanium(IV) isopropoxide. https://www.sigmaaldrich.com/catalog/product/aldrich/377996 (accessed 20/05/2020).
3. Antimony(III) oxide. https://www.sigmaaldrich.com/catalog/product/aldrich/379255 (accessed 20/05/2020).
4. Wu, B. S.; Xu, Y. T.; Bu, Z. Y.; Wu, L. B.; Li, B. G.; Dubois, P., Biobased poly(butylene 2,5-furandicarboxylate) and poly(butylene adipate-co-butylene 2,5-furandicarboxylate)s: From synthesis using highly purified 2,5-furandicarboxylic acid to thermo-mechanical properties. *Polymer* **2014,** *55* (16), 3648-3655, https://doi.org/10.1016/j.polymer.2014.06.052.
5. van der Klis, F.; Knoop, R. J. I.; Bitter, J. H.; van den Broek, L. A. M., The effect of Me-substituents of 1,4-butanediol analogues on the thermal properties of biobased polyesters. *J. Polym. Sci., Part A: Polym. Chem.* **2018,** *56* (17), 1903-1906, https://doi.org/10.1002/pola.29074.
6. Arnaud, S. P.; Wu, L.; Wong Chang, M. A.; Comerford, J. W.; Farmer, T. J.; Schmid, M.; Chang, F.; Li, Z.; Mascal, M., New bio-based monomers: tuneable polyester properties using branched diols from biomass. *Faraday Discuss.* **2017,** *202*, 61-77, https://doi.org/10.1039/C7FD00057J.
7. Rohindra, D.; Lata, R.; Kuboyama, K.; Ougizawa, T., Crystallization behavior in miscible blends of poly(ε-caprolactone) and poly(hexylene adipate) with similar thermal properties studied by time-resolved Fourier transform infrared spectroscopy. *Polym. Cryst.* **2019,** *2* (1), https://doi.org/10.1002/pcr2.10037.
8. Haernvall, K.; Zitzenbacher, S.; Amer, H.; Zumstein, M. T.; Sander, M.; McNeill, K.; Yamamoto, M.; Schick, M. B.; Ribitsch, D.; Guebitz, G. M., Polyol structure influences enzymatic hydrolysis of bio-based 2,5-furandicarboxylic acid (FDCA) polyesters. *Biotechnol. J.* **2017,** *12* (9), https://doi.org/10.1002/biot.201600741.